Distribution, variability and sources of tropospheric ozone over south China in spring: Intensive ozonesonde measurements at five locations and modeling analysis

Yiqiang Zhang,[1,2] Hongyu Liu,[2] James H. Crawford,[3] David B. Considine,[3,4] Chuenyu Chan,[1] Samuel J. Oltmans,[5,6] and Valerie Thouret[7]

[1] We examine the characteristics of the spatial distribution and variability of tropospheric ozone (O_3) by analysis of 93 ozonesonde profiles obtained at five stations over south China (18–30°N) during a field campaign in April–May 2004. We use a global 3-D chemical transport model (GEOS-Chem) to interpret these characteristics and to quantify the sources of tropospheric O_3 over south China during this period. The observed tropospheric O_3 mixing ratios showed strong spatiotemporal variability due to a complex interplay of various dynamical and chemical processes. A prominent feature in the upper and middle troposphere (UT/MT) was the frequent occurrence of high O_3 mixing ratios shown as tongues extending down from the lower stratosphere or as isolated layers at all stations. The model largely captured the observed pattern of day-to-day variability in tropospheric O_3 mixing ratios at all stations, but often underestimated those tongues or isolated layers of O_3 enhancements observed in the UT/MT, especially at low-latitude stations. We found that tropospheric O_3 along the southeast China coast was mainly produced within Asia. Lightning NO_x emissions (over South Asia and equatorial Africa) and/or stratospheric influences were responsible for major events of high O_3 observed in the UT/MT at all stations. Underestimated contributions of these sources likely led to the model's underestimate in the low-latitude UT/MT O_3. This study emphasizes the need for improved understanding of lightning NO_x emissions and stratospheric influences over the Eurasian and African continents and for better representation of these processes in current global models.

1. Introduction

[2] Tropospheric ozone (O_3) is the principal source of the hydroxyl radical (OH) that controls the oxidizing capacity of the atmosphere [*Thompson*, 1992], and is an important greenhouse gas in the upper troposphere (UT) [*Lacis et al.*, 1990]. It is produced by photochemical oxidation of hydrocarbons and carbon monoxide (CO) by OH radicals in the presence of oxides of nitrogen ($NO_x \equiv NO + NO_2$), and is also transported down from the stratosphere. Ozone precursors (NO_x, CO, hydrocarbons) arise from fossil fuel combustion, industrial processes, biomass burning, vegetation, microbial activity in soils, and lightning.

[3] Tropospheric O_3 concentrations and emissions of NO_x have both increased significantly over China as a result of rapid industrialization during the past decade [*Richter et al.*, 2005; *Ding et al.*, 2008; *Wang et al.*, 2009]. These trends degrade local and regional air quality and have important effects on background tropospheric O_3 and surface O_3 over downwind North Pacific and North America [*Jaffe et al.*, 1999; *Jacob et al.*, 1999; *Yienger et al.*, 2000]. *Zhang et al.* [2008] showed that Asian pollution increased surface O_3 concentrations by 5–7 ppbv over western North America in spring 2006. *Cooper et al.* [2010] recently reported an increasing O_3 trend in the western United States lower free troposphere (LT, 3–8 km) on the order of 4–5 ppbv increase

[1]School of Environmental Science and Engineering, Sun Yat-sen University, Guangzhou, China.
[2]National Institute of Aerospace, Hampton, Virginia, USA.
[3]Chemistry and Dynamics Branch, NASA Langley Research Center, Hampton, Virginia, USA.
[4]Now at NASA Headquarters, Washington, D. C., USA.
[5]CIRES, University of Colorado Boulder, Boulder, Colorado, USA.
[6]Global Monitoring Division, NOAA ESRL, Boulder, Colorado, USA.
[7]Laboratoire d'Aerologie, UMR5560, Toulouse, France.

Corresponding author: H. Liu, Chemistry and Dynamics Branch, NASA Langley Research Center, Science Directorate, Mail Stop 401B, Hampton, VA 23681, USA. (hongyu.liu-1@nasa.gov)

per decade when air had a likely origin over eastern Asia. In situ observations of tropospheric O_3 over Asia are therefore essential to testing and improving our understanding of the impact of Asian anthropogenic (versus natural) emissions and various chemical, physical, and dynamical processes on both regional and global tropospheric O_3. Improved understanding will allow better prediction of the effect of future changes in tropospheric O_3 on climate and air quality.

[4] Tropospheric O_3 exhibits high spatial and temporal variability, which can result in large differences in radiative forcing, atmospheric oxidative capacity and air quality [*Ramanathan and Dickinson*, 1979; *Lacis et al.*, 1990]. A wide range of dynamic and chemical processes, such as long-range and regional transport of O_3-rich or O_3-depleted air, stratosphere-troposphere exchange, and photochemical production and loss of O_3, contribute to this variability. The interplay of these processes is inherently complex [*e.g.*, *Cooper et al.*, 2004; *Lin et al.*, 2012], particularly in East Asia [*e.g.*, *Liu et al.*, 2002]. In this paper, we examine the characteristics of the vertical distribution and spatiotemporal variability of tropospheric O_3 as observed at five ozonesonde stations over south China during spring 2004, as well as the consistency of these observations with current understanding of tropospheric O_3 chemistry as represented in a state-of-the-art global three-dimensional (3-D) chemical transport model (GEOS-Chem) [*Bey et al.*, 2001a; *Park et al.*, 2004].

[5] Despite the critical importance of in situ observations of tropospheric O_3 profiles over China, such observations have been few and far between in most of the country. Previously, the most extensive observations along the East Asian coast were from Japanese ozonesonde stations. Only a handful of systematic ozonesonde observations in China have been made. In south China, the Hong Kong Observatory (22.38°N, 114.33°E) has regularly performed monthly ozonesonde soundings since October 1993, and soundings of weekly or higher frequency to support aircraft missions (e.g., NASA PEM-West B, 1994; TRACE-P, 2001) [*Chan et al.*, 1998; *Liu et al.*, 1999, 2002; *Chan et al.*, 2003a, 2003b; *Oltmans et al.*, 2004]. Two other stations in China supported TRACE-P with ozonesonde soundings at Kunming (25.03°N, 102.68°E) and Lin'an (30.30°N, 119.75°E) [*Chan et al.*, 2003b]. During the Pacific Exploration of Asian Continental Emission phase A (PEACE-A) mission in January 2002, ozonesondes were launched at Hong Kong, Beijing (39.81°N, 116.47°E) and Xining, in northwestern China (36.43°N, 101.45°E) [*Chan et al.*, 2004]. Ozonesonde measurements have also been made at Xining in the summer of 1996 [*Zheng et al.*, 2004].

[6] Previous studies showed that tropospheric O_3 has strong geographical variations and differing sources in south and north China. *Chan et al.* [1998] found that tropospheric O_3 over Hong Kong has an obvious springtime maximum and a summertime minimum. A relative minimum of O_3 (30–40 ppbv) in the UT (9–16 km) was frequently observed over Hong Kong in late autumn and winter, as a result of air masses transported from the tropical region by the East Asia local Hadley circulation. *Liu et al.* [1999] hypothesized that large O_3 enhancements accompanied with high humidity at 2–5 km over Hong Kong in spring were due to biomass burning in continental Southeast Asia. This was later confirmed by the TRACE-P ozonesonde and aircraft data [*Chan*

et al., 2003b] as well as modeling analysis [*Liu et al.*, 2002]. *Oltmans et al.* [2004] reported that biomass burning in either Southeast Asia or Africa led to enhanced O_3 layers in the UT over Hong Kong and Taipei during TRACE-P. By analysis of TRACE-P aircraft data, *Liu et al.* [2003] proposed that deep convection plays a more important role than frontal lifting in driving export of biomass burning effluents of Southeast Asia during spring. Stratospheric O_3 was found to be an important source of O_3 in the UT of Xining, Beijing and Hong Kong during PEACE-A [*Chan et al.*, 2004], and of Lin'an during TRACE-P [*Chan et al.*, 2003b]. Lightning NO_x emissions were also found to significantly affect the UT/MT O_3 in subtropical East Asia, especially in winter, spring and fall [*Liu et al.*, 2002]. However, previous in situ O_3 measurements have limited temporal and spatial coverage and are not adequate for a full understanding of the processes controlling the day-to-day variability and sources of tropospheric O_3 over the whole of China.

[7] The springtime maximum of tropospheric O_3 is one of the most distinctive characteristics of the seasonal cycle of O_3 in the Northern Hemisphere, including East Asia [e.g., *Oltmans and Levy*, 1992; *Fishman and Brackett*, 1997; *Logan*, 1999]. Previous studies have proposed different hypotheses to explain the springtime tropospheric O_3 maximum, including stratospheric injection [*Logan*, 1985], tropospheric photochemistry [*Penkett and Brice*, 1986], wintertime accumulation of anthropogenically produced O_3 [*Liu et al.*, 1987] or its precursors [*Honrath et al.*, 1996], and superimposed contributions of O_3 transported from the stratosphere peaking in January–April with O_3 produced in the troposphere peaking in April–June [*Wang et al.*, 1998]. *Stohl et al.* [2003] suggested that stratospheric injection may be the cause of springtime O_3 maximum in the UT but cannot be the cause of the late spring O_3 maximum in the LT. By analysis of ozonesonde data obtained during TRACE-P, *Oltmans et al.* [2004] proposed that the prominent spring maximum throughout the troposphere over East Asia is tied to the location of the jet stream and its influence on stratosphere-troposphere exchange, as well as the increase in photochemical O_3 production through the springtime. Biomass burning emissions in continental Southeast Asia are maximum in spring and make a major contribution to the excessive springtime O_3 in the troposphere over south China [*Liu et al.*, 1999, 2002; *Chan et al.*, 2003a, 2003b; *Lin et al.*, 2009]. However, there is still no consensus as to the origins of the springtime tropospheric O_3 maximum over East Asia. Some issues such as quantification of the stratospheric input and the role of long-range transport versus in situ photochemical production of O_3 warrant further study [e.g., *Monks*, 2000].

[8] To investigate the ensemble of processes that control the distribution, variability, and sources of springtime tropospheric O_3 over China and its surrounding regions, an intensive ozonesonde sounding campaign, called Transport of Air Pollutants and Tropospheric Ozone (O_3) over China (TAPTO-China), was conducted at nine locations across China in the spring of 2004 (south China) and 2005 (North China). The major objectives of TAPTO-China were: (1) To determine the springtime vertical distribution of O_3 in the troposphere over China in order to understand the ensemble
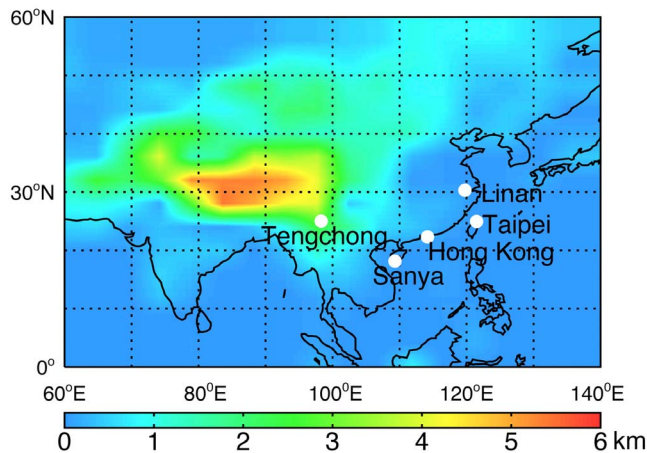
Figure 1. Locations of the five ozonesonde stations in south China during the first phase of the TAPTO-China ozonesonde campaign (April–May, 2004): Sanya (18.14°N, 109.31°E), Hong Kong (22.31°N, 114.17°E), Taipei (24.95°N, 121.49°E), Tengchong (25.01°N, 98.30°E), and Lin'an (30.30°N, 119.75°E). Surface topography is shown as color image.

of processes that control its distribution; (2) To explore the extent of springtime surface O$_3$ pollution in China and assess the processes that control O$_3$ formation and transport; and (3) To characterize the transport of O$_3$ and pollution from upwind source regions of the Eurasian and Southeast Asian subcontinent and quantify its impact on the distribution of tropospheric O$_3$ over China and its outflow to the Pacific.

[9] In this paper, we use the GEOS-Chem model to examine the characteristics of the distribution, variability and various sources of tropospheric O$_3$ over East Asia by analysis of intensive in situ ozonesonde data obtained at five stations in south China during the first phase of TAPTO-China (April–May 2004). The paper is structured as follows. The ozonesonde measurements and the GEOS-Chem model are briefly described in section 2. We discuss the meteorological features of East Asia during April–May, 2004 in section 3. Characteristics of the distribution and variability of springtime tropospheric O$_3$ over south China in both the ozonesonde observations and the model are examined in section 4. Model analyses of the sources of tropospheric O$_3$

are presented in section 5, followed by summary and conclusions in section 6.

2. Data and Methods

2.1. Ozonesonde Measurements

[10] Figure 1 shows the locations of the five ozonesonde stations in south China during the first phase of the TAPTO-China ozonesonde campaign (April–May, 2004): Sanya (18.14°N, 109.31°E), Hong Kong (22.31°N, 114.17°E), Taipei (24.95°N, 121.49°E), Tengchong (25.01°N, 98.30°E), and Lin'an (30.30°N, 119.75°E). Table 1 summarizes the number of ozonesonde soundings available at each ozonesonde station. These ozonesonde stations cover the regions extending from the edge of tropics in the most southern Chinese province of Hainan Island to subtropical southwestern China close to the Southeast Asian border, along the East Asian coast to southeastern China in the industrialized Pearl River Delta and the Taipei metropolitan area to the edge of middle latitudes in central eastern China within the well-developed Yangzi River Delta. On average, one ozonesonde sounding was performed every 2–3 days for each ozonesonde station and a total of 93 soundings were acquired during the experiment period of TAPTO-China 2004. This is the first time that intensive soundings have been conducted simultaneously at several locations covering such a large region in south China.

[11] Our balloon-borne soundings used ozonesondes accompanied with a Global Positioning System radiosonde capable of measuring the wind vector. The O$_3$ sensor was an Electrochemical Concentration Cell (ECC/SPC-6A for Hong Kong and Taipei and ECC/EN-SCI model 2Z for other ozonesonde stations). The sounding system consisted of a Vaisala RS-80 403 MHz radiosonde and an electronic interface connecting signals from the ozonesonde to the radiosonde. The sondes were packaged and flown with a 1200 g rubber balloon (Totex 1200) that normally attained maximum altitudes of 30–35 km within 1.5–2 h. The average ascent rate of the balloon and sensors was about 350–400 m/minute. The values of atmospheric O$_3$ partial pressure, ambient pressure, temperature and relative humidity were telemetered back to a Kenwood receiving system or a Vaisala MW 15 receiving system (for ECC/SPC-6A) and recorded by a computer. The whole ozonesonde and radiosonde system and the preparation procedures for the ECC sensors

Table 1. Number of Ozonesonde Soundings at Five Stations in South China During April–May, 2004

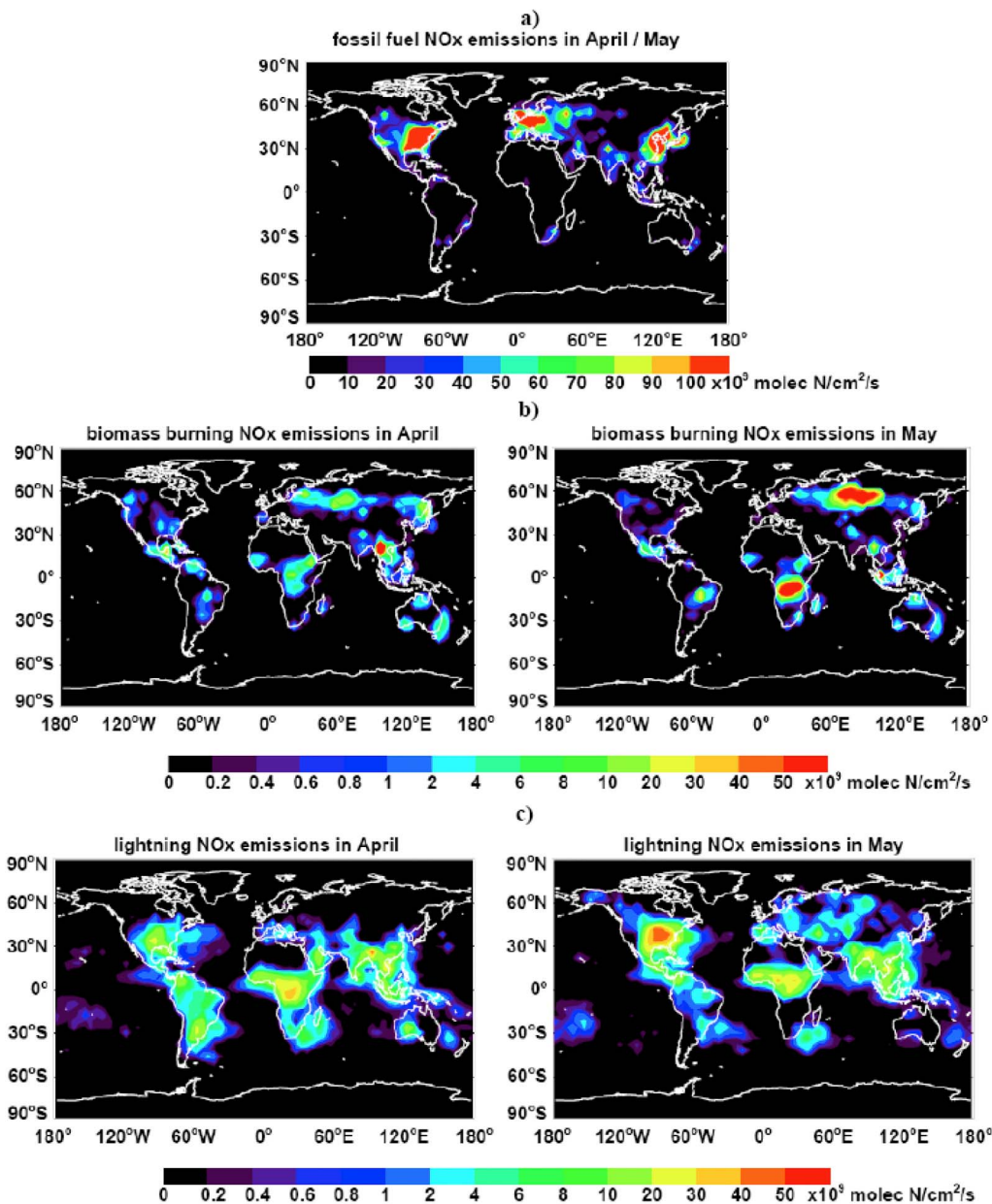| Station	Latitude, Longitude	Altitude (m ASL)	Location	Period of Measurements	Number of Soundings
Sanya	18.14°N, 109.31°E	6	Sanya Upper Meteorological Station in Sanya City, Hainan Island	April 2-May 21	23
Hong Kong	22.31°N, 114.17°E	66	King's Park Upper Meteorological Station in metropolitan Hong Kong, to the south of the Pearl River Delta	April 2-May 14	19
Taipei	24.95°N, 121.49°E	11	Panchiao Upper Meteorological Station in a rural area of Taipei City	April 2-May 3	14
Tengchong	25.01°N, 98.30°E	1655	Tengchong Upper Meteorological Station in a semi-rural area of Tengchong County, Yunnan Province on the southeastern edge of the Tibetan Plateau	April 5-May 19	19
Lin'an	30.30°N, 119.75°E	96	Lin'an Regional Air Quality Monitoring Station in a rural village on the western side of the Yangzi River Delta	April 5-May 19	18

Figure 2. (a) Fossil fuel, (b) biomass burning, and (c) lightning NO_x emissions for April and May 2004 in the model. Fossil fuel NO_x emissions are seasonally invariant.

used at Hong Kong and the stations in mainland China were similar to those we previously used in the spring of 2001 during the TRACE-P period [*Chan et al.*, 2003b] and PEACE aircraft missions [*Chan et al.*, 2004]. The sensors used at Taipei were similar to those described in *Liu and Chang* [2001] and *Oltmans et al.* [2004]. The soundings were usually launched at 1300–1400 local time at Sanya, Hong Kong and Lin'an, 1100–1200 local time at Tengchong, and 0900–1400 local time in Taipei.

[12] The accuracy of ECC ozonesonde O_3 measurements is estimated to be about 10% in the troposphere, except in the case of very low mixing ratios (<10 ppbv) where the accuracy drops to 15% [*Oltmans et al.*, 1996]. The comparisons described in the WMO/GAW (Global Atmospheric Watch) report suggest that the ENSCI-Z type ozonesonde

has accuracies of ±3–4% below 20 km and ±5–10% between 20 and 35 km [*Smit and Sträter*, 2004]. The average response time for the ECC sensor is 27 ± 2 s. The ECC-6A type ozonesonde has almost the same accuracy [*Smit and Sträter*, 2004]. Although it has been found that interfering species, such as NO_2 and SO_2, also react with the potassium iodide (the reacting agent in the ECC sensor) [*Schenkel and Broder*, 1982], their concentrations are usually in a range where they are expected not to constitute a significant impact on the O_3 data. All raw ozonesonde data are sampled every 2 or 15 s, and are averaged every 100 m in this study.

2.2. Model Simulations

[13] GEOS-Chem is a global 3-D model of tropospheric chemistry driven by assimilated meteorological observations
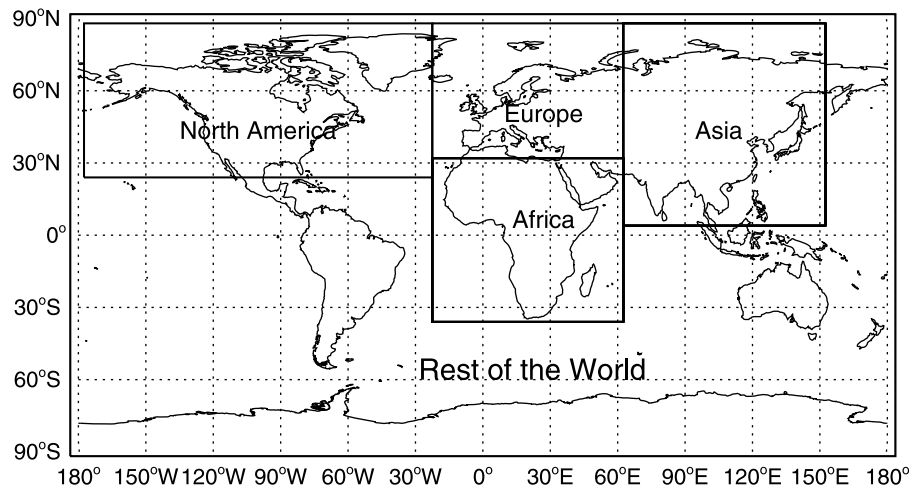
Figure 3. Tropospheric source regions used for tagged O_3 simulations.

from the Goddard Earth Observing System (GEOS) of the NASA Global Modeling and Assimilation Office (GMAO). We use here GEOS-Chem version 8-02-02 (see http://acmg. seas.harvard.edu/geos/) driven by the GEOS-4 assimilated meteorological fields (at $4° \times 5°$ resolution) for the year of 2004. A brief description of the model, meteorological fields, and emissions used in the model is given in the Appendix.

[14] Figure 2 shows fossil fuel, biomass burning, and lightning NO_x emissions for April and May 2004 in the model. The TAPTO ozonesonde stations are located either within or to the south of the concentrated fossil fuel emissions region in East China (Figure 1). Southeast Asia was one of the regions with the strongest biomass burning emissions in April 2004. Human-initiated agricultural burning and forest fires in Southeast Asia usually reach their full strength in the dry season of late winter and spring (February–April) [*Hao and Liu*, 1994; *Duncan et al.*, 2003], peaking in March. Toward May, biomass burning in Southeast Asia decreases substantially. There is also significant biomass burning over equatorial and northern sub-Saharan Africa, Siberia and Northeast China in April. Fires over Siberia increase tremendously in May. Biomass burning over southern Africa is also rather strong in May, but since they are located in the Southern Hemisphere, they have little impact on south China. Strong lightning NO_x emissions occur in regions which are upwind of south China (North Africa, India, Bay of Bengal, Indochina Peninsula, south China Sea) as well as the lower-latitudes of south China.

[15] To investigate the contributions to tropospheric O_3 concentrations over south China from different source regions in the model, we decompose O_3 (actually odd oxygen) into tagged tracers that originate from production in those source regions [*Wang et al.*, 1998]. The tagged tracers are removed (via chemical loss and dry deposition) at the same frequencies as those for total O_3. We archived daily 3-D fields of O_3 production and loss rates from the standard full-chemistry simulation for the year 2004. This tagging approach has been used previously in a number of studies [e.g., *Liu et al.*, 2002, 2009]. It is noted that tagging O_3 by source regions does not describe the sensitivity of O_3 to emissions in that region because of chemical nonlinearity and transport of O_3 precursors from region to region. Figure 3

shows the tropospheric source regions used in this study for tagged O_3 simulations. Ozone produced in the stratosphere is tagged as a separate tracer. The sum of all the tagged O_3 tracers replicates the results from the standard full-chemistry simulation.

[16] To examine the sensitivity of tropospheric O_3 over south China to various emissions, we also conduct model sensitivity simulations where emissions from a given source type or region, including Asian fossil fuel, European fossil fuel, North American fossil fuel, biomass burning, and NO_x from lightning, are suppressed. All sensitivity simulations are conducted for the same period (April and May 2004), and with the same 8-month initializations as for the standard full-chemistry simulation. By subtracting the results of each sensitivity simulation from those of the standard full-chemistry simulation, we estimate the impact of each corresponding source on the tropospheric O_3 over south China during April–May, 2004.

[17] We calculate backward air trajectories with the NOAA Climate Monitoring and Diagnostic Laboratory 10-day isentropic back trajectory model [*Harris and Kahl*, 1994], which uses gridded meteorological analyses produced by the European Center for Medium Range Weather Forecasts. The input meteorological data has a spatial resolution of 2.5 degrees and a temporal resolution of 12 h. The modeled trajectories are believed to give a reasonable representation of large-scale circulations.

3. Meteorology of East Asia During April–May, 2004

[18] Spring in Asia is a period of meteorological transition between the winter and summer monsoons. Figure 4 shows monthly averaged wind vectors over East Asia in the lower troposphere (LT, 878 hPa), the middle troposphere (MT, 515 hPa) and the UT (193 hPa) for April and May 2004. Also shown as color images is the geographic distribution of simulated O_3 mixing ratios in GEOS-Chem. The Siberian High weakens in April and May and the strength of the winter monsoon winds and the frequency of cold surges decrease, but the LT over North China is still dominated by north-westerly winds, as far south as 35°N (Figure 4). By contrast,
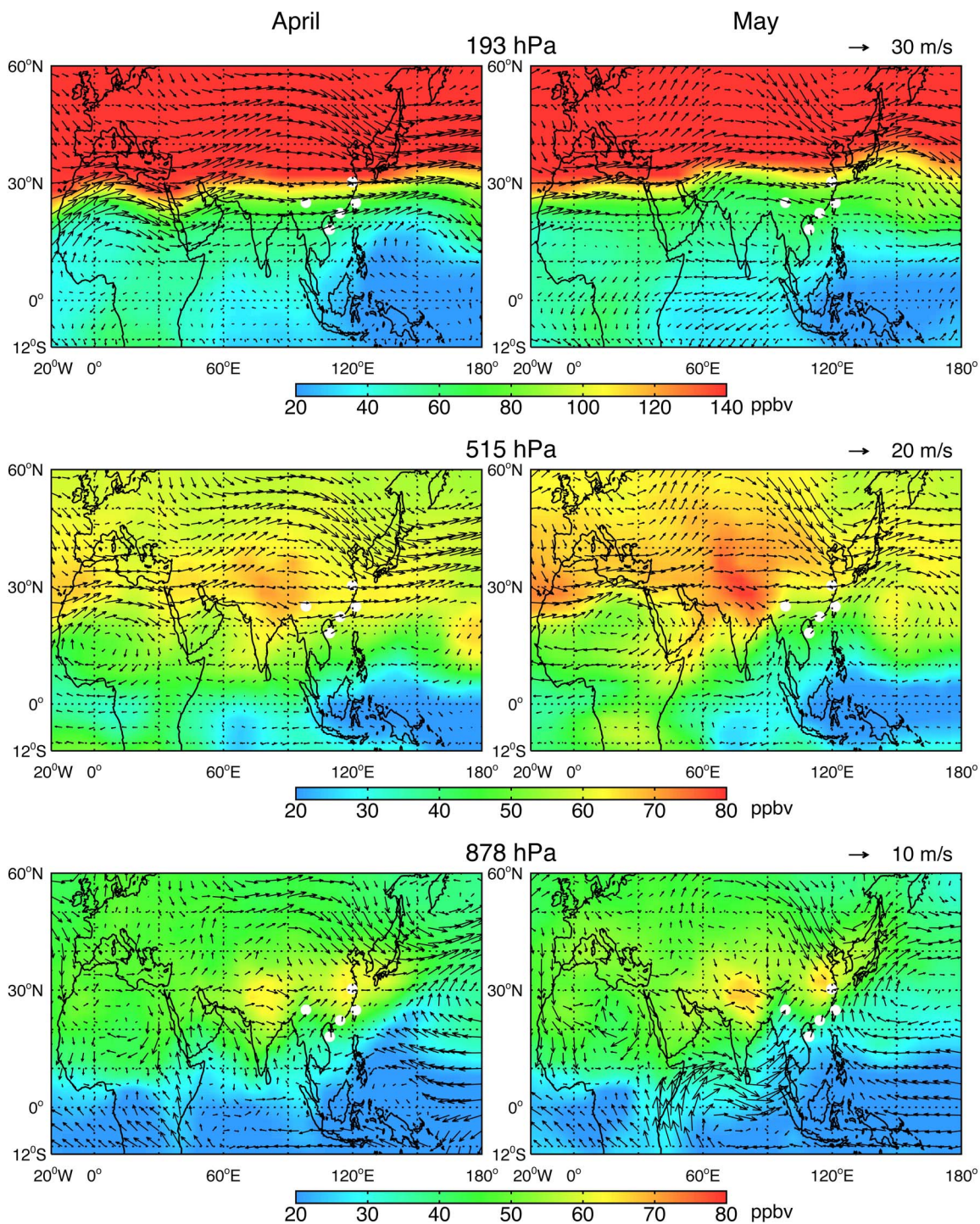
Figure 4. GEOS-4 horizontal wind vectors over East Asia for (left) April and (right) May 2004 in the lower troposphere (LT, 878 hPa), the middle troposphere (MT, 515 hPa), and the upper troposphere (UT, 193 hPa). Also shown as color images are the GEOS-Chem simulated ozone mixing ratios (ppbv). Values are monthly averages. White dots indicate the locations of five ozonesonde stations (Figure 1). Note that color is saturated at 140 ppbv in the top panel.

incursions of warmer tropical air from the south become more frequent. Southwesterly winds prevail in the LT over south China (as far north as 30°N), including the Tengchong, Hong Kong and Sanya ozonesonde stations. These air masses travel over the Bay of Bengal and the Indochina Peninsula,

more rapidly in May when the East Asian summer monsoon starts to develop [*Ding and Chan*, 2005]. Figure 4 shows the presence of a convergence zone over central/eastern China near 30°N with mixed wind direction and lower wind speed, where air masses from the north and the south encounter each
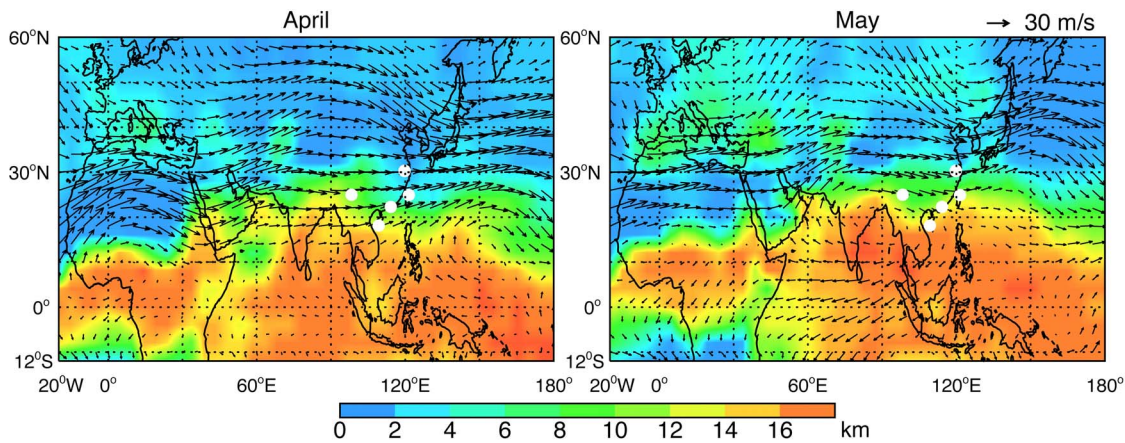
Figure 5. GEOS-4 convective cloud top height (images) and horizontal wind vectors (193 hPa) in April and May, 2004. White dots indicate the locations of five ozonesonde stations (Figure 1).

other. The Lin'an ozonesonde station is located in this region and under the influence of both northerly and southerly winds. Vertical transport associated with this convergence zone plays an important role in the export of pollution from the Asian continent to the western Pacific in spring [*Bey et al.*, 2001b]. On the other hand, Southeast China, including Sanya, Hong Kong and Taipei, is under the influence of southerly and southeasterly winds from the south China Sea and the western Pacific, especially in May when the western Pacific subtropical high gets stronger and closer to the East Asian coast (Figure 4). Taipei is however influenced not only by southwesterly winds but also northerly winds during the transition period in spring [*C. Y. Lin et al.*, 2010]. Relatively high O_3 mixing ratios (~60 ppbv) in the model LT are seen in North India and East Asia, where there are large anthropogenic emissions (Figure 2).

[19] In the MT, northwesterly winds still prevail in North China and westerly winds dominate south China. The model shows high O_3 mixing ratios (~70 ppbv) over the Tibetan Plateau in April, with a higher value in May (~80 ppbv) (Figure 4). The latter is probably associated with intense STE found around the Tibetan Plateau and increased photochemical production of O_3 toward late spring. In their model, *Hsu et al.* [2005] found that the STE is most intense around the 20°N–40°N latitude belt of the Tibetan Plateau in May compared to the rest of the year. They argue that this phenomenon is clearly associated with the transition of the subtropical jet moving poleward and the rise of the tropopause on the anticyclonic side of the jet [*Robinson*, 1980]. In the UT, strong westerly or northwesterly winds dominate East Asia. The Japan jet stream intensifies over eastern China and Japan and weakens in the western Pacific, with its core lying at about 30°N–35°N and maximum wind speed ~40 m/s. The South Asia High starts to establish in the UT over the oceans to the East Philippines in April, and moves northwestward and lies above the Bay of Bengal in May. The spatial distribution of O_3 shows a strong meridional gradient in the UT over the subtropics, reflecting the transition from the (higher) tropical tropopause to the (lower) midlatitude tropopause.

[20] Figure 5 shows the GEOS-4 convective cloud top height (CTH) in April and May, 2004. Convection was strongest at Sanya among all five stations, with CTH about 14 km in both April and May. Convection was weakest at Lin'an. Overall convection in south China intensified and extended northward in May as the Asian summer monsoon set in. Convection can lift surface ozone and its precursors up to the free troposphere while it may also increase O_3 in the free troposphere via convectively induced lightning NO_x emissions. However, water vapor-rich and O_3-depleted air masses in the tropics near the Maritime Continent are frequently lifted upward into the UT by deep convection, and then transported northward along the upper-branch of the eastern Asian local Hadley circulation leading to low O_3 concentrations in the UT over East Asia, especially south China [*Chan et al.*, 1998].

4. Characteristics of Distribution and Variability of Tropospheric Ozone Over South China

[21] In this section we examine the characteristics of the distribution and variability of springtime tropospheric O_3 over south China in both the ozonesonde observations and the model and evaluate how the meteorological circulation patterns at different vertical levels affect the overall shape of O_3 vertical profiles. Previous multiyear records of O_3 mixing ratios in the LT over East Asia, including Hong Kong and Taipei, have exhibited variations that were significantly different from those in the MT/UT [*Oltmans et al.*, 2004]. We thus discuss ozonesonde O_3 observations in the LT (0–4 km) and then the middle (4–8 km) and upper (8 km-tropopause) troposphere, followed by model results for the five ozonesonde stations. The low-latitude stations are discussed first. Figure 6 compares the observed and simulated average profiles of O_3 mixing ratios and corresponding standard deviations for each station during April–May 2004. Figure 7 shows the time-height cross-sections of ozonesonde-observed O_3 mixing ratios and simultaneously measured relative humidity (RH). Figure 8 shows the time-height cross-sections of GEOS-Chem simulated O_3 mixing ratios and GEOS-4 RH at the time (day) and location corresponding to ozonesonde measurements. The GEOS-4 and sonde thermal tropopause heights as defined by the World Meteorological Organization (WMO) are comparable overall (Figures 7 and 8). Ozonesonde
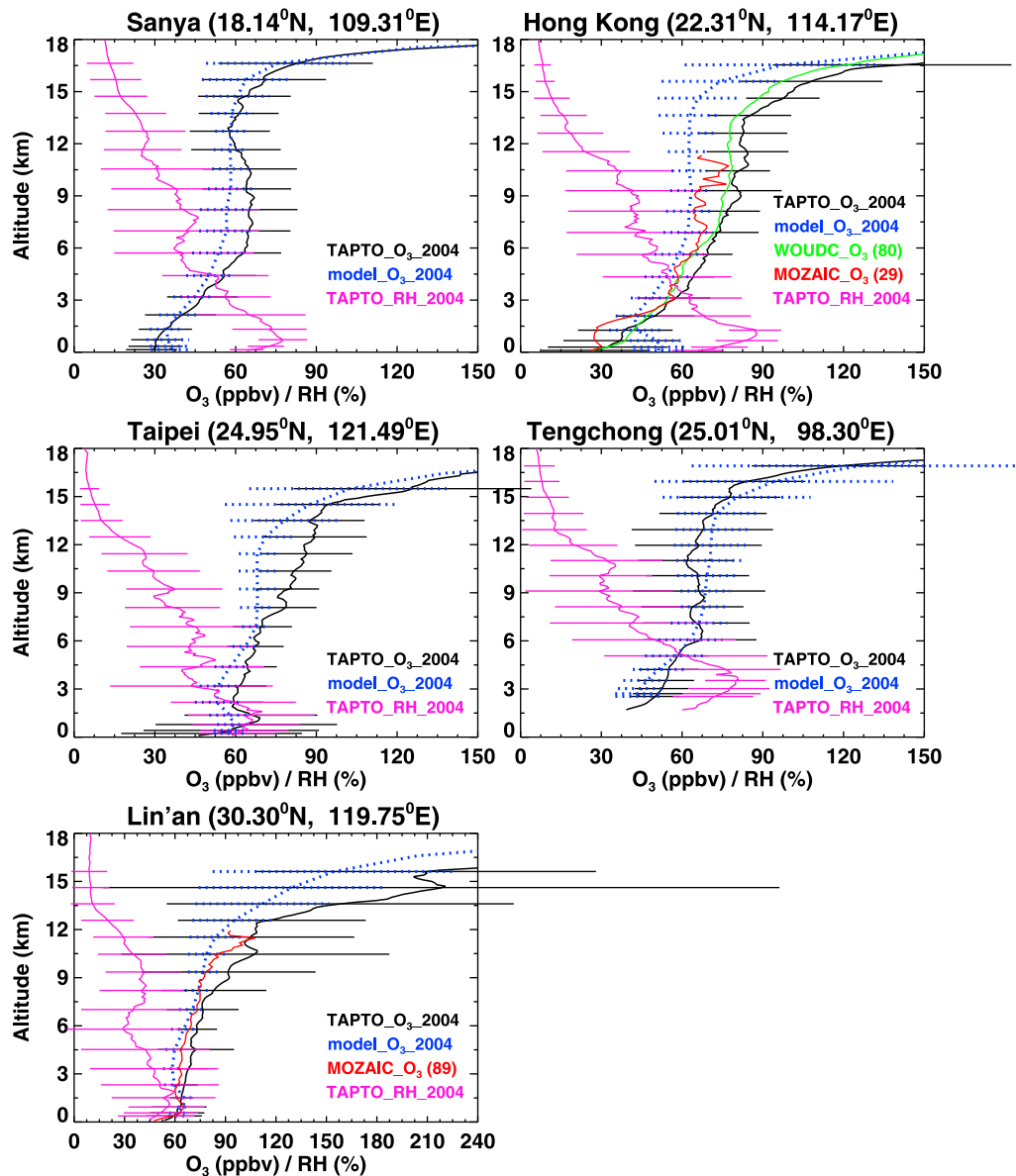
Figure 6. Ozonesonde mean vertical profiles of ozone mixing ratios (solid lines) in comparison with model simulations (dashed lines) during April–May, 2004. Daily model output was sampled at the time (date) and location of each ozonesonde sounding. Sonde-observed mean relative humidity is shown as magenta solid lines. Horizontal lines indicate standard deviations at the altitudes of model vertical levels. Also shown in the panels for Hong Kong and Lin'an are the climatologically averaged O_3 profiles determined using the WOUDC database or from the MOZAIC aircraft measurements. The MOZAIC mean profile in the Lin'an panel is for Shanghai ($\sim$200 km from Lin'an).

observed and model simulated tropospheric O_3 mixing ratios and standard deviations for each station are summarized in Table 2. Sampling the model output at higher temporal resolution or at adjacent grid-boxes does not affect the results significantly.

4.1. Lower-Tropospheric Ozone From Ozonesonde Observations

[22] *Sanya.* Located near the South China Sea and at the lowest latitude, the Sanya station is affected most by clean maritime air masses from tropical regions (Figure 4). This

was reflected by 29 ± 10 (mean $\pm$ standard deviation) ppbv of average O_3 mixing ratio observed near the surface, the lowest among all five stations, with an increasing trend in the LT (Figure 6). The vertical extent of low O_3 mixing ratios ($\sim$30 ppbv) extended to $\sim$2 km before April 26 and up to $\sim$4 km thereafter (Figure 7). This abrupt increase in the vertical extent of low O_3 is attributed to the fact that the earliest onset of the East Asian summer monsoon is usually observed in late April and early May in the Indochina Peninsula [*Ding and Chan*, 2005], followed by northward advancement to the Bay of Bengal and eastward to the south
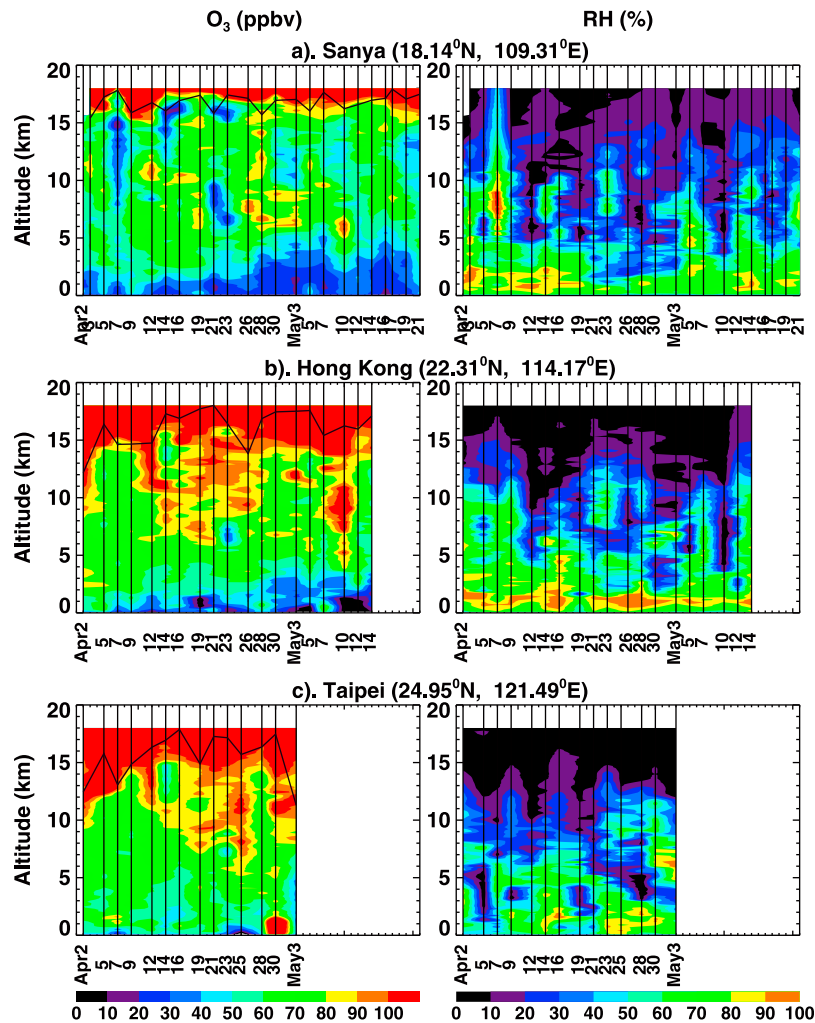
Figure 7. Time-height cross-sections of tropospheric ozone mixing ratios (ppbv) and relative humidity (%) as observed by ozonesondes at five stations in south China (Figure 1) during April–May 2004. Note the different color scale in the panel for O$_3$ at Lin'an. Vertical lines indicate dates with ozonesonde launchings. Horizontal lines indicate thermal tropopause heights based on the WMO definition. White space denotes missing data.

China Sea in mid-late May (Figure 4). The onset of the summer monsoon resulted in more clean and moist maritime (cloudy) air and thus low O$_3$ accompanied by rather high RH (>60%) in the LT over Sanya.

[23] *Hong Kong.* Similar to Sanya, the Hong Kong station is affected by clean maritime air masses from tropical regions (Figure 4). The average O$_3$ mixing ratio near the surface was 28 ± 20 ppbv with an increasing trend in the LT (Figure 6). The average O$_3$ mixing ratios in the LT over Hong Kong were 5–10 ppbv lower than those ozonesonde observations during TRACE-P (March 2-April 25, 2001) [see *Chan et al.*, 2003b, Figure 2]. Lower O$_3$ levels during TAPTO 2004 were likely due to the more frequent intrusion of clean, moist maritime air associated with the onset of Asian summer monsoon in late April–early May 2004; the latter was reflected in high RH in the LT and the vertical extent of low O$_3$ concentrations (∼40 ppbv) increasing with time at Hong Kong (as at Sanya, Figure 7). Low values extended to 1.5 km before April 30 and 3.5 km thereafter.

Ozone concentrations near the surface were about 17 ppbv lower than the average surface O$_3$ concentrations measured at a relatively remote coastal site (Cape D'Aguilar, Hong Kong) during February–April 2001 (TRACE-P) [*Wang et al.*, 2003]. The lowered urban O$_3$ concentrations were due to chemical titration by NO$_x$ from vehicular sources, as is commonly observed [*Chan et al.*, 1998]. The titration effect may explain those extremely low-O$_3$ regimes (<10–15 ppbv) clearly discernable near the surface in Hong Kong on April 19, May 3–5, and May 10–12 (Figure 7). These extremely low O$_3$ levels combined with relatively high O$_3$ mixing ratios (∼60–70 ppbv) observed near the surface in early April, April 28 and May 7 are responsible for the large standard deviation (20 ppbv) of O$_3$ near the surface.

[24] Ozone enhancement layers with mixing ratios as high as 138 ppbv (50–75% RH) were previously observed in the LT (2–5 km) at Hong Kong in spring as a result of biomass burning in continental Southeast Asia [*Liu et al.*, 1999; *Chan and Chan*, 2000]. In April–May 2004, only a few cases of
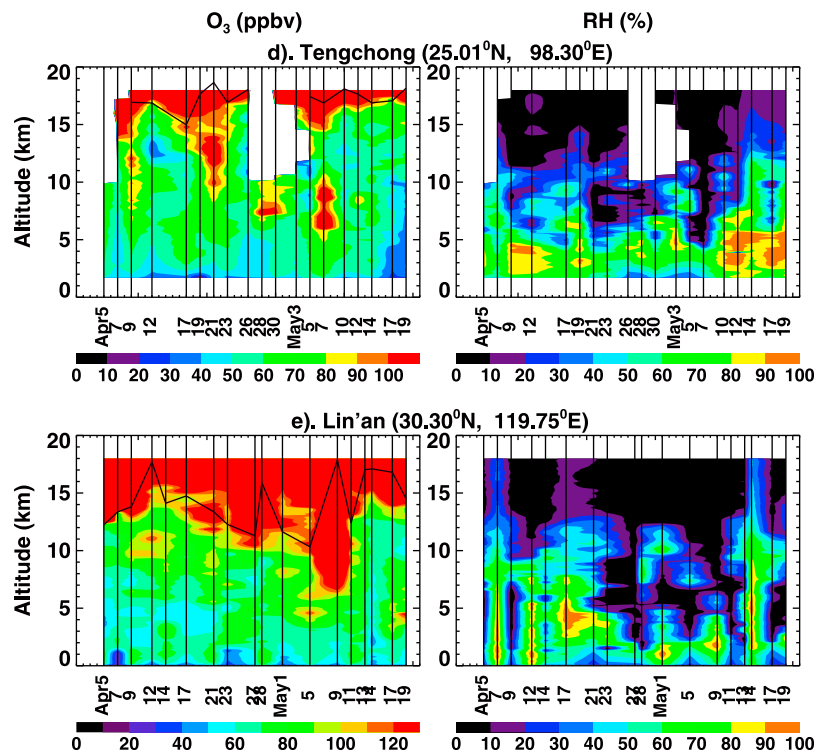
Figure 7. (continued)

such layers (e.g., April 2 and 5), which were much less distinguishable, could be identified. On April 2, high O_3 mixing ratios of ~90 ppbv (RH > 80%) were observed at 2–4 km over Hong Kong. While biomass burning in continental Southeast Asia peaks in March, it remains active and affects tropospheric O_3 over south China in early April.

[25] *Taipei.* The average O_3 mixing ratio near the surface at Taipei (46 ± 34 ppbv) was much higher than at Sanya and Hong Kong (Figure 6). Elevated-O_3 episodes with mixing ratios over 70 ppbv were often seen in the LT (Figure 7), resulting in a distinct local O_3 peak (69 ppbv) at 1.2 km in the average profile (Figure 6). These episodes occurred in the continental outflow of pollution with prevailing northeasterly winds (high O_3 and low RH, e.g., April 16) or under stagnant weather conditions when local pollution accumulated in the LT (high O_3 and high RH, e.g., April 30) [*C. Y. Lin et al.*, 2010]. While Taipei was occasionally impacted by moist marine air masses, it was more frequently influenced by dry continental outflow compared to Sanya and Hong Kong.

[26] *Tengchong.* The average ozone mixing ratio near the surface at Tengchong (1655 m asl, Table 1) was 39 ± 12 ppbv (Figure 6). Surface O_3 levels measured on the top of a mountain (1960 m asl) nearby during TAPTO were overall low compared to those at stations of similar longitude in Southeast Asia and the northeastern Plateau [*Chan et al.*, 2006]. As with other stations along the coast, Tengchong is under the influence of southwesterly clean, moist maritime air masses from the Bay of Bengal, associated with the onset of the Asian summer monsoon (e.g., low O_3 and high RH in April 9–12, April 26-May 3, and

May 17–19). The average O_3 mixing ratios near the surface at Tengchong were lower than at Taipei but higher than Sanya and Hong Kong. This probably reflects less anthropogenic influence at Tengchong than at Taipei and less oceanic influence than at the other two stations.

[27] *Lin'an.* The average O_3 mixing ratio near the surface of Lin'an was the highest (54 ± 15 ppbv) among all five stations (Figure 6). It was close to values (~50 ppbv) measured at this station during TRACE-P [*Chan et al.*, 2003b; *Wang et al.*, 2004]. Frequent outbreaks of elevated-O_3 episodes ([O_3] > 70 ppbv) were observed in the LT (Figure 7). Such episodes were also observed during TRACE-P and resulted mainly from anthropogenic emissions in East China [*Chan et al.*, 2003c]. The overall lowest RH (as low as ~10%) in the LT over Lin'an among all five stations suggested that northerly transport and/or subsidence may also lead to O_3 enhancements at this station. Occasional invasions of clean oceanic air (e.g., April 7 and May 1) were also apparent.

4.2. Mid- and Upper-Tropospheric Ozone From Ozonesonde Observations

[28] *Sanya.* The tropopause over Sanya was the highest among the five ozonesonde stations (~17 km, typical of the tropical tropopause). The average O_3 at Sanya in the FT was the lowest, with an enhancement layer between about 5 km and 12 km (Figure 6). Ozone mixing ratios from 54 ± 12 ppbv at 4 km to 64 ± 17 ppbv at 6 km, remained at ~65 ppbv between 6 and 10 km, and decreased to a minimum of 57 ± 15 ppbv at 12.9 km, followed by substantial increases above. There were cases of high-O_3
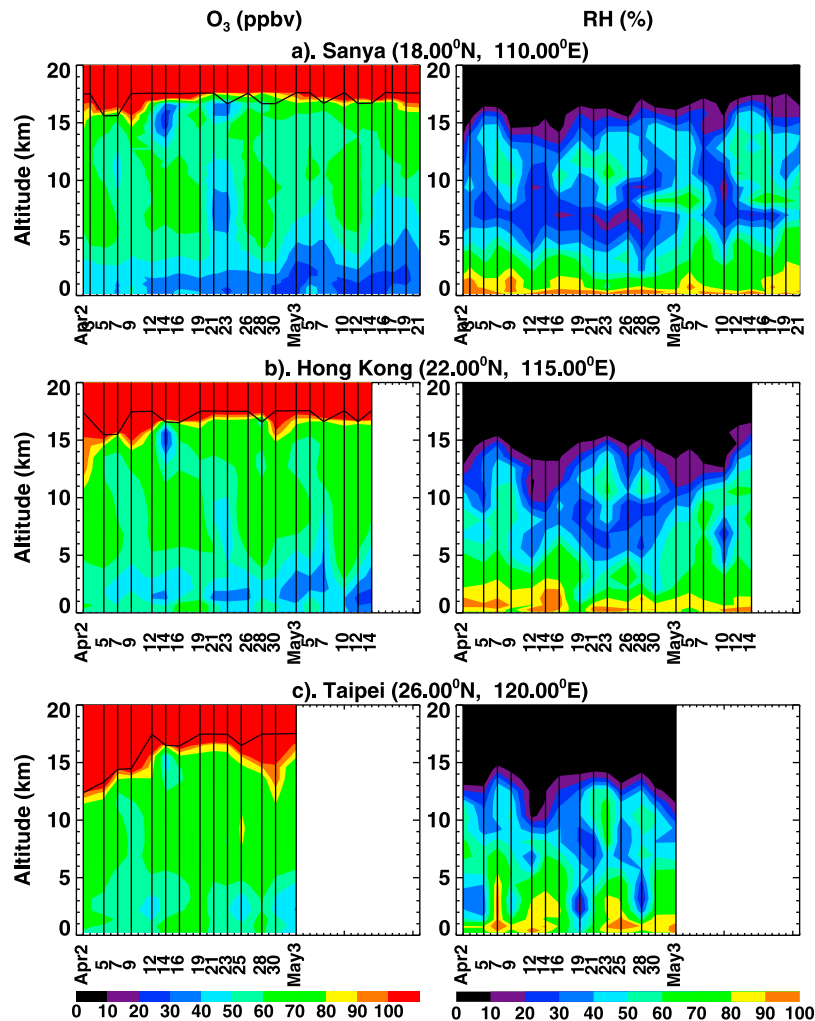
Figure 8. Same as Figure 7, but for (left) daily averaged O_3 mixing ratios (ppbv) and (right) relative humidity (%) in the model. The model results are sampled in the grid point nearest to each station for the corresponding dates (vertical lines) with ozonesonde launchings. Also shown are thermal tropopause heights (black curves) based on the WMO definition.

abundances with low RH especially in the MT (Figure 7), suggesting frequent intrusions of dry air masses with high O_3 from the UT and lower stratosphere (LS). For example, peak O_3 mixing ratios were as high as 100 ppbv at 6–9 km during April 26-May 3 and at 5–7 km on May 10, while the corresponding RH was only ~10% (Figure 7). On the other hand, there were cases of low O_3 abundances (<20–40 ppbv) associated with moist oceanic air (e.g., 8–15 km on April 7, ~16 km on April 21 and 23). Similar low O_3 values in the UT were previously observed at Hong Kong in spring and winter and were attributed to the transport of O_3-depleted tropical marine air in the upper branch of the East Asia local Hadley circulation [*Chan et al.*, 1998; *Liu et al.*, 2002; *Chan et al.*, 2003b]. On April 14, abnormally low O_3 mixing ratios were simultaneously observed in the UT (~15 km) over Sanya, Hong Kong and Taipei. *Chan et al.* [2007] reported that this low O_3 episode resulted from deep convective pumping of low O_3 maritime air masses near the center of typhoon Sudal. The low-O_3 abundances described above were largely responsible for the low average O_3 in the FT (Figure 6).

[29] *Hong Kong.* The O_3 mixing ratios in the FT over Hong Kong were substantially higher than those over Sanya, with O_3 increasing from 63 ± 9 ppbv at 4 km to 83 ± 14 ppbv at 13.4 km, followed by rapid increases above (Figure 6). Much higher O_3 in the FT over Hong Kong was due to the fact that more high-O_3 tongues extended down from the LS and that isolated layers with high-O_3 abundances were frequently observed in the MT/UT over Hong Kong. For example, elevated-O_3 abundances (90 ppbv or higher) were observed in the MT/UT on April 12, 19, 26 and May 10, all accompanied with low RH (~10%). However, a high-O_3 tongue down to 9 km on April 2 and high O_3 in the UT (8–12 km) on April 21–23 were characterized by high RH (~50–70%). Such high-O_3 abundances resulted in average O_3 concentrations above 8 km over Hong Kong in April–May 2004 that were ~5 ppbv higher than the climatological April–May average from the long-term (2000–2009) ozonesonde sounding data obtained from World Ozone and Ultraviolet Radiation Data Centre (WOUDC) (Figure 6). If only April is considered, the excess would be about ~10 ppbv. This excess of O_3 would be even higher compared
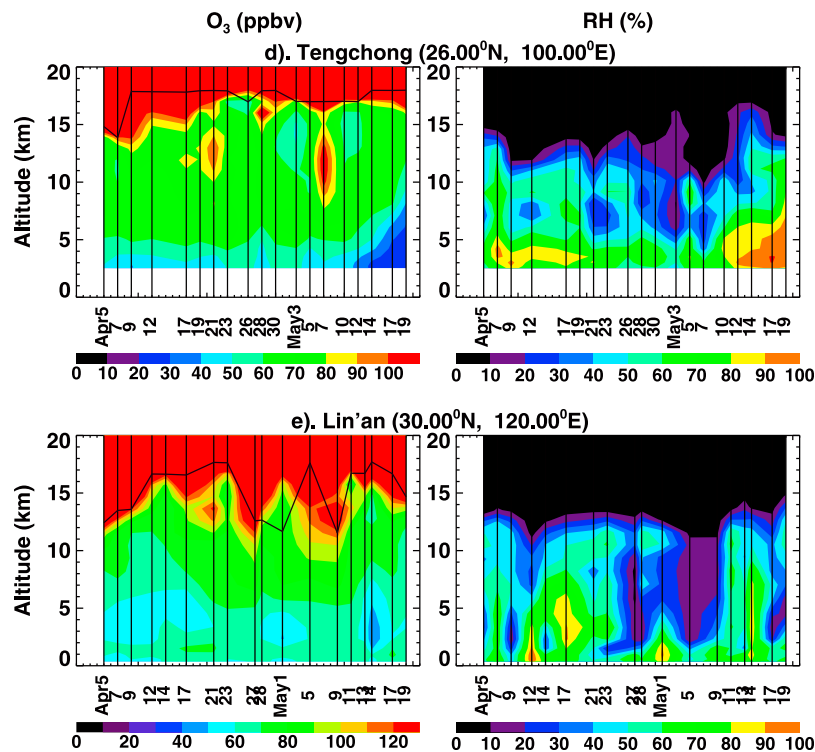
Figure 8. (continued)

to the climatological average profiles (1999–2005) from the Measurement of Ozone by Airbus In-Service Aircraft project (MOZAIC) (Figure 6).

[30] *Taipei.* The average O_3 in the FT over Taipei exhibited a larger vertical gradient than that over Hong Kong. It increased from 64 ± 11 ppbv at 4 km to 92 ± 19 ppbv at 14.5 km, followed by sharp increases above. As at Hong Kong, two high-O_3 tongues (>100 ppbv) extending down from the LS on April 2 and 12, and high-O_3 abundances on April 19 were all characterized by low RH (<20–30%), suggesting possible influences from the UT/LS. By contrast, two other high-O_3 tongues on April 25 and 30 were accompanied by high RH (~60%) (Figure 7), indicating these air masses were likely associated with convection. The enhanced-O_3 abundances (~70–80 ppbv) at 3–6 km during April 25–30 were all characterized by very low RH (~10%), indicating influences from subsiding motions.

[31] *Tengchong.* The observed average O_3 mixing ratios at Tengchong (~60–80 ppbv) exhibited a smaller vertical gradient in the MT/UT, with an O_3 enhancement layer between 6 km and 10 km (Figure 6). The standard deviations in the MT/UT over Tengchong were generally larger than Sanya, Hong Kong and Taipei, reflecting the particularly high O_3 concentrations during the O_3 episodes observed at this station (Figure 7). For example, a high-O_3 tongue during April 7–9 penetrated deeply down to ~6 km, while another high-O_3 tongue of larger spatial scale during April 19–21 penetrated down to ~8 km with maximum O_3 levels of >100 ppbv. Two high-O_3 episodes occurred in the MT during April 28–30 and on May 7, with peak O_3 over 110 ppbv and 150 ppbv, respectively. All the peak O_3

levels above were accompanied by extremely low RH (<~10%), suggesting influences from the UT/LS. Two cases of low-O_3 abundances (~30 ppbv) were found at ~13 km on April 12 and at ~11 km on May 5, respectively, presumably due to convection.

[32] *Lin'an.* At this northernmost station (tropopause at ~13 km), the MT/UT O_3 over Lin'an featured the strongest vertical gradient with an increasing trend with altitude (Figure 6). The average O_3 mixing ratios remained ~70–75 ppbv from 4 km to 7.5 km and then increased to 108 ± 46 ppbv at 12.4 km, with a local peak (109 ± 82 ppbv) at 10.6 km. When compared to the April–May O_3 profile climatology at the nearby Shanghai metropolitan region (31.14°N, 121.79°E), as determined by MOZAIC (1997–2006), O_3 mixing ratios in most of the troposphere (especially the MT/UT) over Lin'an during April–May 2004 were ~5–20 ppbv higher (Figure 6). Since the 89 MOZAIC profiles were obtained in multiple years and should better represent the full range of tropospheric O_3 concentrations than the less frequent sondes in 2004, this bias likely reflects the interannual variability. The remarkably large standard deviations of O_3 mixing ratios in the UT reflected the large variability of O_3 resulting from frequent intrusions of stratospheric O_3 due to the station's proximity to the Japan jet stream. Isolated layers with high-O_3 abundances were also frequently observed in the FT over Lin'an (Figure 7). High-O_3 abundances at 8–10 km on April 21 were accompanied by relatively high RH (~60%). By contrast, high-O_3 abundances at ~10 km during April 9–14, at 8 km on May 1, at 5 km on May 5 and at 3–5 km during May 17–19 were characterized by very low RH (<10–20%). High-O_3 tongues

Table 2. Ozonesonde Observed and GEOS-Chem Simulated O_3 Mixing Ratios (Mean ± Standard Deviation, ppbv) in the Upper, Middle and Lower Troposphere (UT/MT/LT), and Sources of O_3 as Indicated by the Model Tagged O_3 and Sensitivity Simulations at Five Stations in South China During the Ozonesonde Sounding Days of April–May, 2004[a]

Station		UT					MT					LT			
		SY	HK	TP	TC	LN	SY	HK	TP	TC	LN	SY	HK	TP	TC	LN
Ozonesonde		60 ± 16	83 ± 16	86 ± 17	69 ± 20	107 ± 57	63 ± 13	70 ± 9	67 ± 10	68 ± 30	73 ± 12	40 ± 13	50 ± 14	59 ± 11	55 ± 11	65 ± 8
Model		58 ± 6	62 ± 8	68 ± 7	71 ± 14	84 ± 15	54 ± 10	59 ± 9	64 ± 5	66 ± 11	65 ± 8	39 ± 7	42 ± 7	53 ± 8	51 ± 10	60 ± 6
Tagged O_3[b]	Total	56 ± 7	61 ± 9	67 ± 7	72 ± 15	85 ± 17	52 ± 9	56 ± 9	62 ± 5	66 ± 11	65 ± 8	36 ± 5	39 ± 6	53 ± 9	49 ± 10	60 ± 7
	AS	35 ± 10	30 ± 8	25 ± 8	22 ± 12	23 ± 7	33 ± 5	33 ± 5	31 ± 6	27 ± 6	26 ± 8	26 ± 3	27 ± 4	35 ± 7	26 ± 3	38 ± 11
	ST	4 ± 5	8 ± 8	12 ± 7	19 ± 17	30 ± 17	4 ± 3	6 ± 4	9 ± 3	12 ± 6	11 ± 3	2 ± 1	3 ± 2	4 ± 2	7 ± 3	5 ± 1
	AF	8 ± 5	12 ± 5	15 ± 4	14 ± 4	13 ± 2	7 ± 5	8 ± 4	9 ± 2	12 ± 5	8 ± 2	2 ± 2	1 ± 2	1 ± 1	5 ± 2	1 ± 1
	EU	<1	<1	<1	<1	1 ± 1	1 ± 1	<1	2 ± 1	2 ± 2	5 ± 3	<1	<1	3 ± 3	2 ± 1	6 ± 4
	NA	1 ± 1	1 ± 1	2 ± 1	2 ± 1	4 ± 1	1 ± 1	2 ± 2	4 ± 2	5 ± 3	7 ± 3	<1	1 ± 1	4 ± 3	3 ± 2	6 ± 3
	ROW	7 ± 4	9 ± 3	12 ± 3	12 ± 5	14 ± 3	6 ± 2	6 ± 2	7 ± 2	8 ± 2	7 ± 2	3 ± 1	3 ± 1	3 ± 1	5 ± 2	3 ± 1
Sensitivity (delta O_3)[c]	NoASFF	7 ± 2	6 ± 2	5 ± 2	4 ± 2	5 ± 1	8 ± 2	8 ± 2	7 ± 2	5 ± 2	7 ± 2	7 ± 2	8 ± 3	14 ± 5	6 ± 1	16 ± 7
	NoBB	3 ± 1	3 ± 1	3 ± 1	2 ± 1	2 ± 0	3 ± 2	4 ± 2	3 ± 1	3 ± 2	2 ± 1	3 ± 3	4 ± 2	2 ± 1	3 ± 3	2 ± 1
	NoLNOx	18 ± 4	18 ± 4	18 ± 3	16 ± 2	16 ± 3	14 ± 3	14 ± 3	12 ± 3	12 ± 3	9 ± 2	8 ± 2	6 ± 2	3 ± 2	7 ± 2	2 ± 1
	NoEUFF	<1	<1	<1	<1	<1	<1	<1	<1	<1	1 ± 1	<1	<1	1 ± 1	<1	2 ± 1
	NoNAFF	<1	<1	<1	<1	<1	<1	<1	<1	1 ± 1	2 ± 1	<1	<1	1 ± 1	<1	2 ± 1

[a]UT: ~12 km (model vertical Level 13, ~220 hPa); MT: ~6–7 km (model vertical Level 8, ~510 hPa); LT: ~2.2 km for SY/HK/TP/LN and ~4.2 km for TC (model vertical Level 5, ~790 hPa). See Figure 1 for the locations of ozonesonde stations: Sanya (SY), Hong Kong (HK), Taipei (TP), Tengchong (TC), and Lin'an (LN).

[b]Tropospheric source regions (Figure 3) used for tagged O_3 simulations include Asia (AS), Africa (AF), Europe (EU), North America (NA), and the rest of the world (ROW). Ozone produced in the stratosphere (ST) is tagged as a separate tracer.

[c]Decreases in O_3 concentrations when Asian fossil fuel emissions (NoASFF), global biomass burning emissions (NoBB), global lightning NO_x emissions (NoLNOx), European fossil fuel emissions (NoEUFF), and North American fossil fuel emissions (NoNAFF) were turned off.

(>120 ppbv) from the LS were often observed in the UT near tropopause over Lin'an, for example, down to 12 km and 10 km on April 21 and 27–28, respectively. In particular, a remarkable high-O_3 tongue with low RH (∼10%) penetrated deeply down to ∼6 km from the LS on May 9.

[33] The most striking features of tropospheric O_3 distributions at these stations were the frequent occurrences of elevated-O_3 layers, in particular in the UT/MT. Most of these layers were characterized by low RH (<10–20%), implying that they may have recently originated from the UT/LS. These layers were distinct from the O_3-rich biomass burning plumes with moderate RH (50–75%) commonly observed at 2–4 km altitudes during the late winter and spring over subtropical south China and northwestern Pacific [*Liu et al.*, 1999; *Chan et al.*, 2003a, *Oltmans et al.*, 2004], including the cases at Hong Kong on April 2 and 5, 2004.

4.3. Tropospheric Ozone From Model Simulations

[34] *Sanya.* The model underestimates the average MT O_3 observations by ∼15 ppbv with better agreement in the LT and UT (Figure 6). The simulated day-to-day pattern is generally similar to the observations at Sanya (Figures 7 and 8). The model captures well the vertical extent of low O_3 (high RH) in the LT and its temporal evolution, as observed during TAPTO. It also reproduces the observed low-O_3 abundances in the FT on April 7, 14 and 21–23, but not during May 19–21 (Figure 8). Meanwhile, similar to the observations, the RH in the UT on April 7 and 21–23 is relatively high (∼60%), suggesting influences of maritime air masses in the model. However, the high-O_3 abundances observed in the MT/UT are not well reproduced by the model. For example, the model simulates the O_3 enhancements observed at 6–11 km during April 12–19, at 6–9 km during April 26–30 and at 5–7 km on May 10, but with O_3 concentrations ∼20 ppbv lower than the observations (Figure 8). Similar to the observations, the O_3 enhancement on May 10 is accompanied by low model RH (∼20%), indicating transport of air masses from the UT/LS.

[35] *Hong Kong.* The model significantly overestimates the observed O_3 near the surface. This would be expected if the low O_3 is due to local NO_x titration, because such an effect would not be resolved by the model (Figure 6). In the FT, the model underestimates the observations by ∼15–25 ppbv, with biases increasing with altitude. It generally simulates well the vertical extent of low O_3 (high RH) in the LT and its temporal evolution during TAPTO (Figures 7 and 8). Observed high-O_3 tongues or layers are generally captured by the model but with ∼20 ppbv lower concentrations during April 2, 12–19, 26–28 and May 10. For April 21–23, the model fails to reproduce the elevated-O_3 abundances at 9–13 km but shows high RH as observed. As at Sanya, the O_3 enhancement (with low RH) on May 10 is captured qualitatively by the model.

[36] *Taipei.* The simulated O_3 mixing ratios are ∼10 ppbv lower between 1 and 7 km and ∼15–25 ppbv lower between 7 and 14 km, respectively, than the observations (Figure 6). The high-O_3 tongues over Taipei on April 2, 12 and 30 are reproduced by the model, but do not penetrate as deeply as in the observations (Figures 7 and 8). The model simulates well the UT O_3 minimum on April 14 and captures the O_3 enhancements (high RH) in the MT/UT on April 25; in the

latter case, the model O_3 concentrations are ∼20 ppbv too low.

[37] *Tengchong.* The model underestimates the observed average O_3 in the LT by ∼10 ppbv, but reproduces the observations in the MT/UT without biases (Figure 6). Low O_3 concentrations in the LT associated with maritime air masses are generally simulated well but the low-O_3 abundances observed at ∼13 km on April 12 are not reproduced by the model (Figures 7 and 8). The model captures the high-O_3 events during April 19–21, 28–30, and May 7 but shows weaker enhancement. The May 7 event in the model occurs at a level ∼2 km above the observations, probably due to the coarse resolution of the model. Consistent with the observation, the low RH accompanied with these O_3 enhancements in the model suggests influences from the UT/LS. The model is less successful in simulating the April 9 event.

[38] *Lin'an.* The model simulates well the observed average O_3 near the surface, but underestimates it in the FT with biases of ∼10 ppbv at 2–8 km and ∼15–20 ppbv above 8 km (Figure 6). The model captures the dry high-O_3 tongues extending from the stratosphere on April 21, 27–28, and May 5–9 (Figures 7 and 8). But the simulated tongue during May 5–9 does not intrude as deep into the MT as in the observations. As with other ozonesonde stations, most of the isolated thin high-O_3 layers are not reproduced by the model, partly due to the much coarser vertical resolution of the model.

[39] In summary, there are substantial differences in the spatiotemporal distribution and variability of observed tropospheric O_3 at the five stations. While the observed pattern of day-to-day variability is largely captured by the model, the latter often underestimates the large enhancements of O_3 seen in the observations, especially at low-latitude stations. However, the distribution and variability of the model RH are generally similar to those observed, suggesting a reasonable representation of convective transport and large-scale ascending and descending motions. Underestimated contributions from lightning NO_x emissions and/or stratospheric O_3 are likely responsible for the model deficiencies at low latitudes, which we will discuss in section 5.

5. Sources of Tropospheric Ozone Over South China During April–May, 2004

[40] We examine in this section the relative contributions to tropospheric O_3 over the TAPTO ozonesonde stations of different source types and source regions in the GEOS-Chem model. Such a comparison will provide clues to the factors controlling tropospheric O_3 over the stations, as well as facilitate identification of model weaknesses in its physical and chemical process representation. Figure 9 shows the contributions to O_3 at Sanya, Hong Kong, Taipei, Tengchong and Lin'an from chemical production in the Asian and African troposphere and in the stratosphere, as determined from tagged tracers (section 2.2). The contributions from chemical production in the European and North American troposphere are also shown for Hong Kong, Tengchong and Lin'an. Figure 10 shows the changes in O_3 concentrations at the five stations when Asian or European or North American fossil fuel, global biomass burning, or lightning emissions were suppressed, as determined from
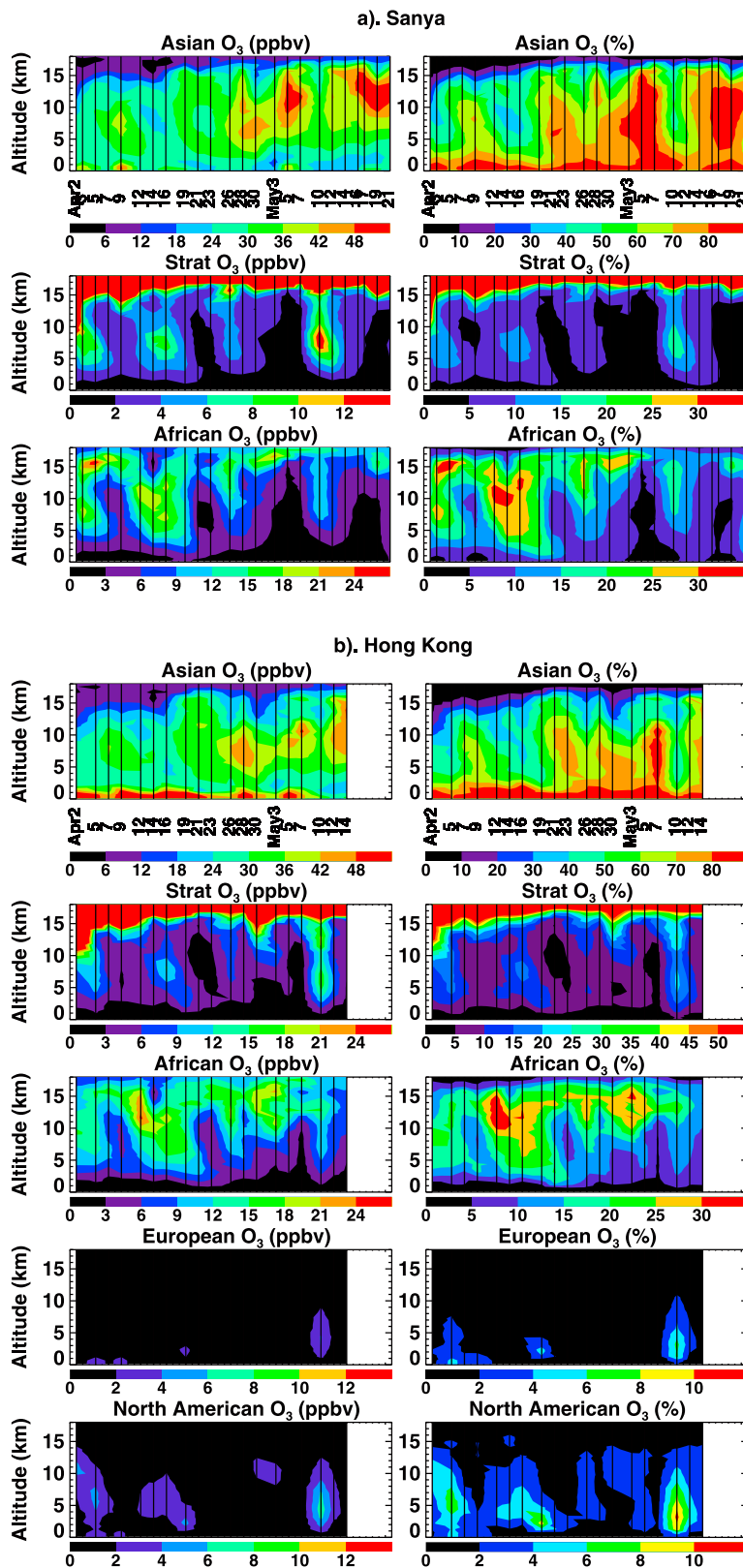
Figure 9. Major source regions for ozone at (a) Sanya, (b) Hong Kong, (c) Taipei, (d) Tengchong, and (e) Lin'an as a function of altitude and date during April–May 2004. The plots show model results for (left) concentrations (ppbv) and (right) percentages (%) of tagged O_3 produced in the Asian and African troposphere (and European, North American troposphere for Hong Kong, Tengchong, and Lin'an) and transported from the stratosphere. Model daily output is sampled at the time (date, vertical lines) and location of ozonesonde soundings (see Figures 7 and 8).
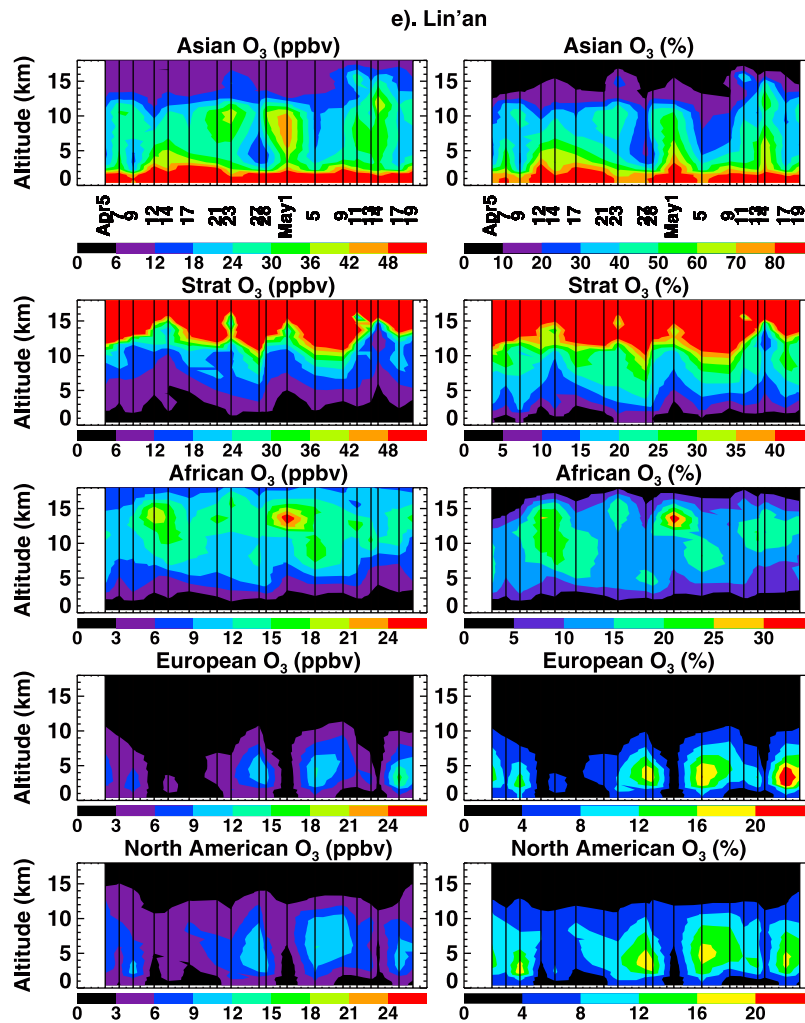
Figure 9. (continued)

Figure 9. (continued)

sensitivity simulations. Table 2 summarizes the contributions to tropospheric O_3 over the stations from different source regions and types based on the tagged O_3 and sensitivity simulations. In this context we analyze the sources of tropospheric O_3 over south China. We focus on the overall distribution and variability, instead of individual events which will be analyzed and reported separately.

5.1. Asian Pollution and Biomass Burning

[41] At Sanya, Hong Kong and Taipei, O_3 between 0 and 2 km was predominantly (~80%) produced within Asia (i.e., "Asian O_3") throughout April–May (Figure 9). When Asian fossil fuel emissions were suppressed, O_3 concentrations decreased by 12 ± 5 ppbv (33%), 26 ± 7 ppbv (51%), and 28 ± 5 ppbv (48%) near the surface at the three stations, respectively (Figure 10). Since these three stations were frequently influenced by monsoonal air masses from tropical marine regions, such large decreases in O_3 concentrations suggest that the air masses had experienced mixing with Asian pollution before reaching these stations. In the MT/UT, "Asian O_3" accounted for a smaller fraction but remained the dominant component most of the time. This is consistent with the model results of *Sudo and Akimoto* [2007], who

showed that O_3 vertical profiles over the Japan and China coast regions during TRACE-P are largely controlled by O_3 production within Asia. The model indicates a substantial increase in the "Asian O_3" starting late April, reflecting enhanced convective transport of O_3 and its precursors as well as lightning emissions associated with convection (Figure 9). Asian fossil fuel emissions increased O_3 by 6–9 ppbv (9–15%) in April and by 9–15 ppbv (15–27%) toward May, with the largest effect often corresponding to the observed O_3 enhancement layers (e.g., Hong Kong on April 12, 30 and May 10) (Figures 7 and 10).

[42] At Tengchong, less than 30 ppbv (~60%) of O_3 in the LT was produced within Asia until mid-May when its contribution increased significantly. Without Asian fossil fuel emissions, tropospheric O_3 concentrations decreased by <9 ppbv (<21%) with maximal effects throughout the troposphere during May 10–19 (Figure 10). The latter reflects an increased role for convection as indicated by both the model and observed RH (Figures 7 and 8). This is also in line with a study by *Li et al.* [2005] who showed that anthropogenic emissions from northeast India and southwest China were transported to the UT by Asian summer monsoon convection and orographic lifting. The model simulates a

significant impact of the "Asian O_3" and Asian fossil fuel emissions between 5 and 10 km on April 9 and 30, corresponding to the high-O_3 episodes observed by ozonesondes (Figure 7). The much weaker influence of Asian fossil fuel emissions on this station is attributed to its upwind and remote location away from the China East coast, the region of highest emissions.

[43] At Lin'an, O_3 between 0 and 2 km was mostly (>80%) produced in Asia and would decrease by 28 ± 4 ppbv (46%) near the surface if Asian fossil fuel emissions were suppressed (Figure 10). The O_3 decreases were generally 3–12 ppbv (6–18%) above 2 km, with larger effects (9–18 ppbv, 15–27%) in the MT during April 12–17. The stronger influence of Asian pollution on O_3 in the free troposphere occurred during those days with stronger upward (frontal or convective) lifting as seen in the model and observed RH. This is evident during April 21–23 and May 1 when high O_3 concentrations were observed between 7 and 10 km (Figures 7–10).

[44] Biomass burning emissions, in particular those over continental Southeast Asia, also represented a significant contribution to O_3 over south China during April–May, even though the emissions peak in March. At the three low-latitude stations along the East China coast, O_3 concentrations decreased by up to 12 ppbv (24%) at ~3 km (Sanya, Hong Kong) and 6 ppbv (12%) at ~3 km (Taipei), respectively, in early April when biomass burning emissions were suppressed in the model (Figure 10). Such decreases were up to 8–10 ppbv (9–15%) at 5–10 km over these three stations during April 26-May 3. At other times and altitude levels, biomass burning emissions contributed ~3 ppbv (~5%) to background O_3 concentrations except near the surface. In their global model, *Sudo and Akimoto* [2007] also found significant O_3 (up to 5 ppbv) imported to the lower troposphere over the China coast from the Southeast Asian biomass burning region in spring. At Tengchong, biomass burning emissions increased O_3 concentrations in the LT/MT by 4–12 ppbv (6–24%) with a maximum at the surface during April 23-May 3. The surface measurements of O_3 at Tengchong also showed that O_3 was the highest during this period [see *Chan et al.*, 2006, Figure 2], although this is not seen in the ozonesonde observations (Figure 7). At Lin'an, biomass burning emissions increased the ~4 km O_3 by ~5 ppbv (~10%) on May 1 and the background O_3 in the UT by 3 ppbv (~5%) throughout the simulation period.

5.2. Stratospheric Influence

[45] Despite their lower latitude locations, Sanya, Hong Kong and Taipei often encounter O_3 transported from the stratosphere in the model (Figure 9). The stratosphere contributed 8–15 ppbv (10–20%) O_3 in the MT/UT over the three low-latitude stations on April 2–5, 4–10 ppbv (5–20%) on April 12–19 and 26. In particular, the stratosphere contributed 10–18 ppbv (10–25%) O_3 to the May 10 event in the MT/UT over Sanya and Hong Kong. Tengchong and Lin'an are located closer to the center of the subtropical jet and thus more often subjected to the impact of intrusions of stratospheric O_3. At Tengchong, the stratosphere contributed >36 ppbv (>40%) O_3 in the UT on April 17, 21 and May 7 (Figure 9). At Lin'an, the stratosphere contributed >48 ppbv (>40%) O_3 in the UT on April 21, April 27–28 and May 9. High-O_3 layers or tongues were observed by ozonesondes

during all these times (Figure 7 and section 4.2). Overall, the stratosphere contributed 31 ± 18 ppbv (33%) and 20 ± 17 ppbv (24%) O_3 in the UT (~12 km) over Lin'an and Tengchong, respectively, much higher than those for Taipei (13 ± 7 ppbv, 18%), Hong Kong (8 ± 9 ppbv, 12%), and Sanya (4 ± 5 ppbv, 7%). The stratosphere tends to make large contributions to O_3 in regions where the photochemistry is quiescent [*Lelieveld and Dentener*, 2000]. We find that stratospheric O_3 has an important impact on O_3 near the surface at the high-elevation station of Tengchong. The stratosphere contributed 5 ± 3 ppbv (12%) O_3 near the surface, but much less (<3 ppbv or <5%) at other stations. These estimates are likely on the low end because the model may have underestimated the stratospheric contribution (by a factor of <2), which will be discussed in section 5.5.

5.3. Lightning

[46] Lightning NO_x emissions make major contributions to the UT/MT O_3 over south China in April–May. Larger influences were found in the UT over low-latitude stations (Sanya, Hong Kong and Taipei) where deep convection was more frequent (Figure 10). When lightning NO_x emissions were suppressed, O_3 concentrations all decreased by ~18 ppbv (~30%) in the UT (~12 km) over these stations with frequent large decreases (>20 ppbv) (Figure 10). In the MT, the decreases were still large (up to 13–16 ppbv or 20–30%). Most of these air masses impacted by lightning are clearly associated with enhanced O_3 concentrations in the ozonesonde observations (Figures 7 and 10). Examples are 10–15 km over all three stations on April 12, 8–10 km over Sanya on April 30, 10 km over Sanya on May 7, and 8–12 km over Taipei on April 25. At Tengchong, O_3 concentrations decreased by 16 ± 3 ppbv (23%) in the UT (12 km) with decreases often greater than 20 ppbv (27%). While the lightning effect did not always emerge as isolated layers of O_3 enhancements, it clearly played an important role in producing the high-O_3 tongue observed in the UT during April 19–21 (Figures 7d, 9d, and 10d). On April 23, significant lightning influences (~10 ppbv or ~18%) were even seen near the surface (Figure 10d). At Lin'an, the impact of lightning NO_x emissions was the smallest, but still as large as 16 ± 3 ppbv (19%) in the UT (11.6 km) and <6 ppbv (10%) throughout the LT. As with stratospheric influences, these estimated lightning effects are probably biased low because the model may have underestimated the lightning NO_x emissions, which will be discussed in section 5.5.

5.4. Intercontinental Transport

[47] Intercontinental transport of O_3 and its precursors contributes significantly to the inflow and outflow of O_3 over East Asia in spring [e.g., *Bey et al.*, 2001b; *Liu et al.*, 2002; *Oltmans et al.*, 2004; *M. Lin et al.*, 2010]. We discuss here the contributions to tropospheric O_3 over south China during TAPTO from the African biomass burning and lightning NO_x emissions as well as European and North American anthropogenic sources.

[48] *African Influence.* While the fossil fuel emissions were very weak over the African continent, biomass burning activities occurred in equatorial and northern sub-Saharan Africa during TAPTO, especially in April (Figure 2). Moreover, there were strong lightning NO_x emissions associated with deep convection over equatorial Africa in April–
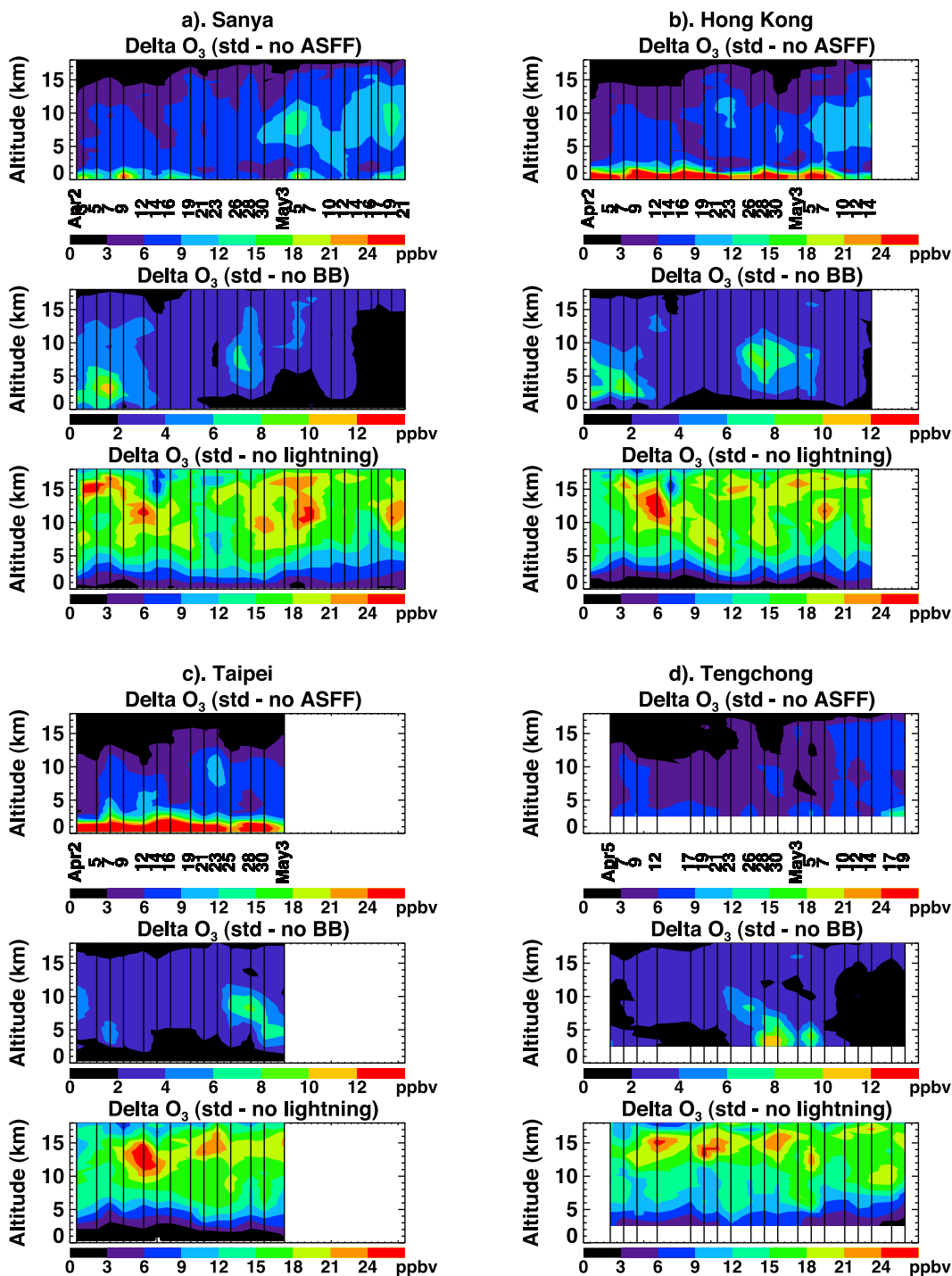
Figure 10. Decreases in tropospheric O_3 concentrations (ppbv) when Asian, European, North American fossil fuel emissions, biomass burning emissions, or lightning NO_x emissions were suppressed, relative to the standard simulation for April–May 2004.
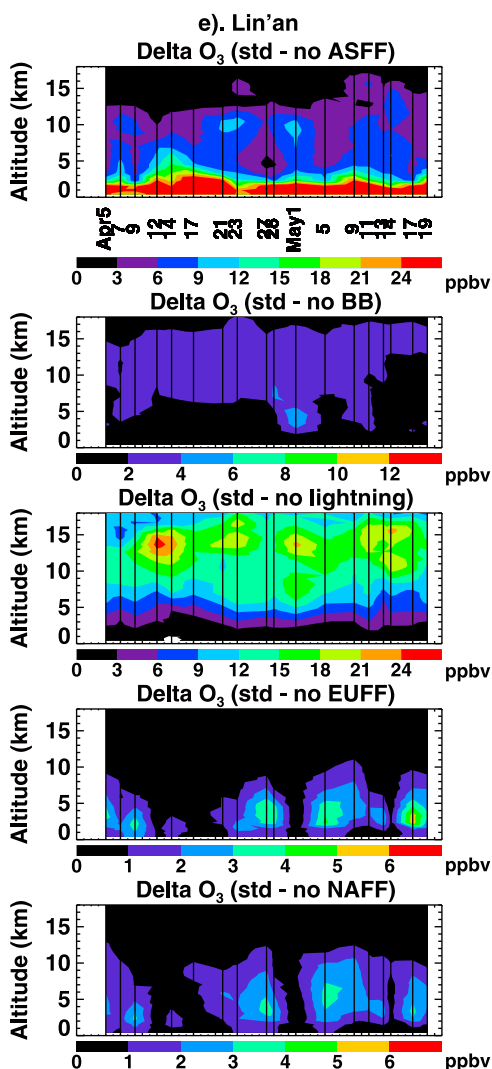
Figure 10. (continued)

May (Figures 2 and 5). Ozone and its precursors from biomass burning emissions convected to the UT, where they were mixed with lightning NO_x emissions, were transported eastward to the downwind regions including south China in the subtropical jet.

[49] At Sanya, Hong Kong and Taipei, about 10–25 ppbv (10–30%) of the UT/MT O_3 originated from the African troposphere (lightning and biomass burning) during April 2–5, 12–19, 26, and May 10 (Figures 9a, 9b and 9c). The frequency of such events decreased in May when convection increased in south China. On April 12, the African troposphere contributed >18 ppbv (>25%) of O_3 to the UT/MT (Figures 9a, 9b and 9c), leading to remarkably strong O_3 enhancements as observed at all three ozonesonde stations (Figures 7a, 7b and 7c). Model sensitivity simulations suggest that African lightning NO_x (versus biomass burning) emissions are the main contributor (Figures 10a, 10b and 10c). Tropospheric O_3 over Tengchong, which is located closest to Africa, was contributed to the most by the African troposphere among all stations. Africa contributed 5 ± 2 ppbv (12%) of O_3 near the surface on average, and ~8 ppbv

(~20%) during April 12–26 (Figure 9d). It often contributed >24 ppbv (>30%) of O_3 in the UT. The simulated African O_3 event in the MT on May 3 corresponds to only moderately enhanced O_3 in the observations (Figures 7d and 9d).

[50] At Lin'an, Africa contributed 9–21 ppbv (15–25%) of O_3 in the MT/UT (Figure 9e). Large contributions occurred in the UT during April 12–14 and May 1, when there were maximum O_3 decreases due to suppressed lightning NO_x emissions. This indicates again the major influence of the African lightning NO_x emissions on tropospheric O_3 over south China. This influence may be even larger since lightning NO_x emissions are likely underestimated in the model, which will be discussed in section 5.5. In a similar context, *Sudo and Akimoto* [2007] found in their model significant long-range O_3 exports from the North African and South American free troposphere, which contribute 3–7 ppbv to the UT O_3 over the Japan and China coast regions in spring.

[51] It is interesting to note that the African O_3 and stratospheric O_3 components in the model at lower-latitude stations (e.g., Sanya and Hong Kong) often positively correlate with each other (Figure 9). By contrast, they tend to negatively correlate at higher-latitude stations (e.g., Tengchong and Lin'an). While the former suggests the mixing of African air masses with stratospheric air on the route to the lower-latitude of south China, the latter implies that stratospheric air masses affecting Tengchong and Lin'an often originated from higher latitudes.

[52] *North American and European Pollution.* European and North American air masses may travel eastward and then downward as part of the large-scale subsiding motion of the anticyclone associated with the Asian winter monsoon, thus affecting East Asia, especially the higher-latitude regions. At Sanya, Hong Kong and Taipei both the North American and European troposphere typically contributed <4 ppbv (<4%) to tropospheric O_3. The contribution was larger when there was concurrent downward transport of air from the UT/LS (Figure 9b). For example, the North American troposphere contributed 4–6 ppbv (~8%) to the LT/MT O_3 at Hong Kong on May 10. At Tengchong, the North American and European troposphere made similar but a few ppbv larger contributions to tropospheric O_3 (Figure 9d). On May 7, the North American troposphere contributed >12 ppbv (16–20%) to the MT (~7 km) O_3 and ~5 ppbv (~10%) to the surface O_3.

[53] The North American and European troposphere contributed most (typically 3–12 ppbv or 4–20%) to tropospheric O_3 at Lin'an, among the five stations (Figure 9e). As with other stations, the North American and European influence usually coincided with subsiding motions or stratospheric influence. During April 27–28, May 5 and 17, both the North American and European troposphere contributed 9–15 ppbv (12–20%) to O_3 at ~5 km, with the combined effect greater than 30%. Interestingly, the simulated stronger events on May 5 and 17 were clearly identified in the ozonesonde observations (e.g., O_3 enhancements at ~5 km on both days, Figure 7e). The model O_3 decreased by 3–5 ppbv (3–9%) when the European or North American fossil fuel emissions were suppressed (Figure 10e).

5.5. Discussion

[54] The model significantly underestimated the MT/UT O_3 observations in south China during TAPTO, especially at
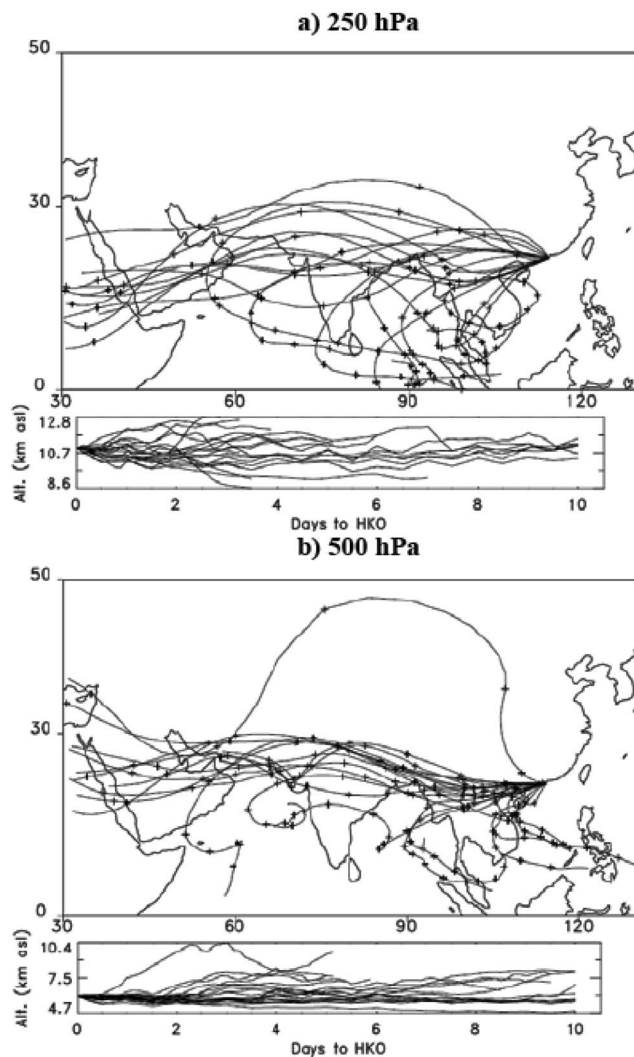
Figure 11. Isentropic 10-day back trajectories arriving at (a) 250 hPa and (b) 500 hPa over Hong Kong during all ozonesonde launching days (April–May, 2004).

low-latitude stations (e.g., Hong Kong, section 4). Tagged tracers and sensitivity experiments suggested that African lightning NO_x emissions merged into the Northern Hemisphere subtropical jet and thus mixed with stratospherically influenced air masses, as they were transported eastward en route to south China (section 5.4). We discuss this further below.

[55] Figure 11 shows the isentropic 10-day back trajectories arriving at 250 hPa and 500 hPa over Hong Kong during all ozonesonde launching days during April–May 2004. The majority of air masses reaching 250 and 500 hPa over Hong Kong have traveled over the subtropical regions of North Africa, the Middle East, the northern India Peninsula and Southeast Asia. The trajectories clearly show that a number of air masses at these altitudes have experienced substantial subsiding motions when they traveled over the above regions. These regions of subsidence are also shown in a plot of the average vertical pressure velocity at 200 hPa during April–May 2004 (Figure 12). The subsidence is associated with the subtropical jet in these regions, and results in downward transport of high O_3 in the UT/LS as

well as noticeable decreases in RH. Tropospheric O_3 measured by the Tropospheric Emission Spectrometer (TES) on the Aura satellite during 2005–2010 also showed that O_3 in the UT over the Middle East is highest with frequent high-O_3 tongues of >100 ppbv extending down to 250 hPa during spring (e.g.,http://tes.jpl.nasa.gov/visualization/SCIENCE_PLOTS/Trends/HTML_Files/Middle_East.html). Such high-O_3 air masses in upwind regions can consequently travel eastward and contribute significantly to tropospheric O_3 in south China. The above analysis is consistent with our GEOS-Chem model calculations with respect to the major contributions of stratospheric O_3 and African lightning NO_x emissions.

[56] The model generally simulated those stratospheric O_3 intrusions much better at Tengchong than at other stations, which largely explains the fact that simulated average O_3 is close to observed O_3 throughout the troposphere over Tengchong. Although the model captures the occurrences of significant stratospheric O_3 intrusions at other stations (section 5.2), the intrusions are usually not as deep as the observations (e.g., Hong Kong, Taipei on April 2 and Lin'an on May 9) or the magnitudes are underestimated (e.g., Hong Kong on May 10). Similarly, the model also underestimated observed O_3 enhancements in isolated layers of stratospheric origin. Therefore, it is likely that stratospheric O_3 contributions were underestimated at these stations. *Hudman et al.* [2004] previously suggested that the Synoz flux boundary condition for cross-tropopause transport of O_3 in GEOS fields provides an effective constraint on the global scale but may underestimate stratospheric influence in regions of preferential downwelling. They showed that the GEOS-Chem model underestimates the stratospheric contribution of O_3 in the troposphere by a factor of 2 when examining Asian and stratospheric influence on O_3 above the west coast of the United States in spring 2002. Scaling up the stratospheric contribution by a factor of 2 in our study would improve the model-observation agreement in the MT over Sanya, the free troposphere over Hong Kong, the MT over Taipei and the free troposphere over Lin'an, but would overestimate O_3 in the UT over Taipei and in the MT/UT over Tengchong (not shown).

[57] Lightning NO_x emissions are highly uncertain and may contribute to the model bias as the dominant contributor to tropical tropospheric O_3 [*Sauvage et al.*, 2007; *Parrington et al.*, 2008]. As discussed in section 5.3, while the model captured the episodes of lightning influences, it often underestimated the corresponding enhancements of ozone mixing ratios. This deficiency suggests that the model likely underestimated the contribution of lightning NO_x emissions, in addition to that of stratospheric O_3. This is in line with an inverse modeling study by *Lin* [2012] who found that a posteriori lightning NO_x emissions are about 18% higher than the a priori estimates. It is also consistent with the study of *Jourdain et al.* [2010] who showed that GEOS-Chem with a value of 6 Tg N yr^{-1} for the lightning source underestimates the O_3 enhancements observed by TES over the USA in July 2006 and suggested that the model constraints on the strength of the lightning NO_x emissions are limited by the fact that the model underestimates the stratospheric influence. In our model, increasing lightning NO_x emissions from ~6 to ~8 Tg N yr^{-1} would improve the model-observation agreement in the MT over Sanya and the free troposphere
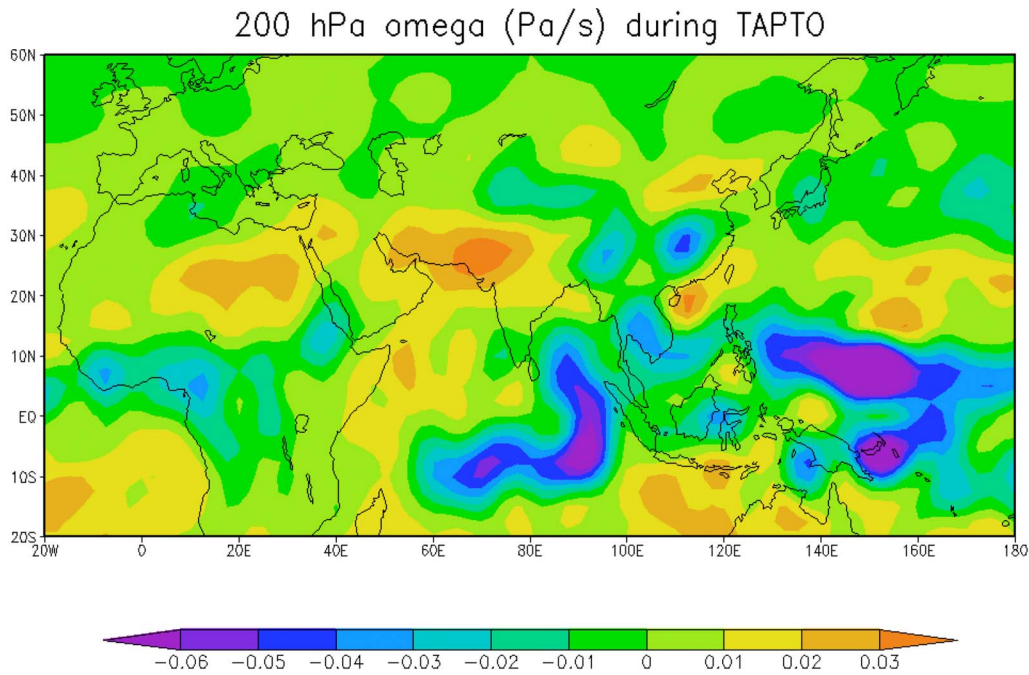
Figure 12. The average vertical pressure velocity (Pa/s) at 200 hPa during TAPTO (April 2-May 21, 2004). Positive and negative values indicate downward and upward motions, respectively. NCEP reanalysis data provided by the NOAA-CIRES/Climate Diagnostics Center (http://www.esrl.noaa.gov/psd/data/ reanalysis/reanalysis.shtml).

over Hong Kong and Taipei, but the model would still significantly underestimate the O_3 in the MT/UT over Hong Kong and the UT over Taipei and would overestimate the O_3 in the MT/UT over Tengchong (not shown).

[58] Model simulations presented in this paper were conducted at a coarse ($4° \times 5°$) horizontal resolution and may have more difficulty in capturing the observed fine-scale O_3 enhancements than higher resolution simulations, thus contributing to the model's underestimate in the UT/MT O_3. However, a standard full-chemistry simulation ($2° \times 2.5°$) using a recent version (v9-01-02) of the model indicates that while it yields slightly better model-observation agreement, our conclusion regarding the model underestimate in the UT/MT O_3 is not affected.

6. Summary and Conclusions

[59] A total of 93 ozonesonde soundings were conducted at five stations over south China (18–30°N) during the first phase of the TAPTO campaign in April–May 2004, providing a unique data set for studying tropospheric O_3 in the region. We have examined the characteristics of the distribution and spatiotemporal variability of the observed tropospheric O_3 mixing ratios. A global 3-D model of tropospheric chemistry (GEOS-Chem) driven by assimilated meteorological data from the NASA Goddard Earth Observing System (GEOS-4) has been used to interpret these characteristics and to quantify the sources of springtime tropospheric O_3 over south China.

[60] The observed O_3 mixing ratios in the lower troposphere (LT) showed similarities as well as substantial differences in the spatiotemporal distribution and variability

among the stations. The intrusion of clean, moist marine air masses of tropical origin resulted in the lowest average O_3 mixing ratios near the surface of Sanya (29 ± 10 ppbv) and Hong Kong (28 ± 20 ppbv). At these low-latitude stations, the vertical extent of low O_3 mixing ratios in the LT increased with time, reflecting the onset of the Asian summer monsoon in late April and May. By contrast, average O_3 mixing ratios near the surface at Taipei (46 ± 34 ppbv) and Lin'an (54 ± 15 ppbv) were much higher, with elevated-O_3 (>70 ppbv) episodes often found in the polluted LT. The intermediate average O_3 mixing ratios (39 ± 12 ppbv) near the surface at Tengchong (southwest China) reflect less influence from both anthropogenic emissions and tropical marine air. Several cases of O_3 enhancement layers in the LT (2–4 km) at Hong Kong, as a result of the biomass burning in continental Southeast Asia, were identified but were much less distinguishable during TAPTO.

[61] The most striking feature in the observed O_3 mixing ratios in the upper and middle troposphere (UT/MT) is the frequent occurrences of high-O_3 tongues extending down from the lower stratosphere (LS) or isolated layers at all stations. Low relative humidity (RH < 10–20%) accompanying most of these tongues or layers suggest that they originated from the UT/LS very recently. While more frequent occurrences of high-O_3 tongues and isolated layers result in higher average O_3 mixing ratios in the free troposphere at Hong Kong and Taipei than those at Sanya, high-O_3 tongues appear to be more intense at the stations of higher latitudes (Tengchong and Lin'an). Low O_3 mixing ratios (<20–40 ppbv) observed in the UT/MT at low latitudes, especially Sanya, usually resulted from the transport of O_3-depleted tropical marine air in the upper branch of the

East Asia local Hadley circulation or associated with deep convective systems (e.g., typhoons) in the western Pacific.

[62] The model largely captures the observed pattern of day-to-day variability in tropospheric ozone mixing ratios at all stations. It simulates well the vertical extent of low O_3 mixing ratios (high RH) in the LT and its temporal evolution at low-latitude stations (Sanya and Hong Kong), as well as those O_3-depleted air masses in the UT/MT associated with tropical deep convection. But the model often underestimates those tongues or isolated layers of O_3 enhancements observed in the UT/MT, especially at low-latitude stations. The distribution and variability of the model RH are generally similar to those observed, indicating a reasonable representation of large-scale and convective transport processes in the model.

[63] We investigated the sources of tropospheric O_3 over the TAPTO ozonesonde stations by tagging O_3 produced from different source regions in the model and by model sensitivity calculations. We found that O_3 in the LT over Sanya, Hong Kong, Taipei and Lin'an was predominantly (~80% or greater) produced within Asia and would decrease by 12–28 ppbv (33–51%) if Asian fossil fuel emissions were suppressed in the model. The weaker influence (<9 ppbv or <21%) of Asian fossil fuel emissions at Tengchong is attributed to its remote location away from the heavily polluted China east coast. In the UT/MT, the contribution of Asian sources remained dominant most of the time. It increased with convective transport of O_3 and/or its precursors from the continental boundary layer as well as associated lightning NO_x emissions toward late April and May. This was more obvious at low-latitude stations. When biomass burning emissions were suppressed in the model, O_3 mixing ratios decreased by 4–12 ppbv (6–24%) in the LT/MT over the stations in early April and late April - early May. Biomass burning emissions increased background O_3 concentrations in the free troposphere by about 3 ppbv (~5%).

[64] Stratospheric influence and lightning NO_x emissions were responsible for major events of high O_3 observed in the UT/MT over south China during TAPTO. The stratosphere made major contributions to O_3 in the UT (~12 km) over Tengchong (20 ± 17 ppbv, 24%) and Lin'an (31 ± 18 ppbv, 33%), two stations located closer to the subtropical jet. The stratosphere had a significant influence on O_3 near the surface of Tengchong (5 ± 3 ppbv, 12%). Stratospheric influence was also important in the UT/MT over low-latitude stations and is determined by southern shifts of the subtropical jet [*Liu et al.*, 2002].

[65] Lightning NO_x emissions in South Asia and equatorial Africa had a major influence on tropospheric O_3 over south China, especially in the low-latitude UT/MT, during TAPTO. When lightning NO_x emissions were suppressed, O_3 concentrations decreased by ~18 ppbv (~30%) in the UT (~12 km) over Sanya, Hong Kong and Taipei. The air masses impacted by lightning were often associated with enhanced O_3 mixing ratios in the ozonesonde observations. We found that the model often captured the occurrences of lightning and stratospheric influence but underestimated the corresponding enhancements of O_3 mixing ratios in the ozonesonde observations, suggesting an underestimate of either or both of these sources in the model. Enhancing the contributions from these sources, however, does not improve

the model simulations at all stations. The North American and European troposphere made significant contributions to O_3 in the lower free troposphere when subsidence of the UT air occurred at higher-latitude stations, especially Lin'an (30°N).

[66] We find that the intensive ozonesonde observations at five stations in south China are qualitatively consistent with current understanding of tropospheric chemistry as represented by the GEOS-Chem model. Using the model at a higher resolution (2°×2.5°) does not alter our conclusions. This study demonstrated how the complex interplay of surface (anthropogenic, biomass burning) emissions, lightning NO_x emissions, stratosphere-troposphere exchange, intercontinental transport, and convective and monsoonal transport determined the distribution and variability of springtime tropospheric O_3 in south China. Improved understanding is needed particularly with respect to lightning NO_x emissions and stratosphere-troposphere exchange over the Eurasian and African continents. Studies that focus on the representation of these processes in current models should be encouraged. Increasing satellite observations (e.g., TES/Aura) and future multiyear intensive ozonesonde measurements in spring and other seasons should also be helpful in further constraining the model. Such improved models will allow better quantitative projections of tropospheric O_3 in south China and the rest of East Asia in the coming decades.

Appendix A: The GEOS-Chem CTM

[67] We drive the GEOS-Chem model with the GEOS-4 assimilated meteorological observations from the Goddard Earth Observing System (GEOS) of the NASA Global Modeling and Assimilation Office (GMAO). The original description and evaluation of GEOS-Chem as applied to tropospheric O_3-NO_x-VOC chemistry was presented by *Bey et al.* [2001a] and a description of the coupled oxidant-aerosol simulation was given by *Park et al.* [2004]. A number of previous studies have applied the model to tropospheric O_3 in various regions of the world, including the Asian and western Pacific [e.g., *Bey et al.*, 2001b; *Liu et al.*, 2002], the Middle East [e.g., *Li et al.*, 2001; *Liu et al.*, 2009], the United States [e.g., *Fiore et al.*, 2002; *Zhang et al.*, 2008; *Hudman et al.*, 2009], the Atlantic [e.g., *Li et al.*, 2002], and the tropics [e.g., *Martin et al.*, 2002; *Nassar et al.*, 2009; *Zhang et al.*, 2011].

[68] Meteorological fields in the GEOS-4 archive have a temporal resolution of 6 h (3 h for surface variables and mixing depths). The native horizontal resolution of GEOS-4 fields is 1° latitude by 1.25° longitude with 55 levels in the vertical between the surface and 0.01 hPa. For computational expediency, we degrade the horizontal resolution to 4° latitude by 5° longitude for input to GEOS-Chem and merge the vertical levels above 50 hPa retaining 30 vertical levels. The non-local mixing scheme, which takes into account the magnitude of the instability, is adopted to simulate the vertical mixing processes in the planetary boundary layer [*Lin and McElroy*, 2010]. Deep convection and shallow convection of GEOS-4 are based on the algorithms of *Zhang and McFarlane* [1995] and *Hack* [1994], respectively.

[69] The GEOS-Chem model includes 87 chemical species and transports 43 chemical tracers to describe tropospheric

O_3-NO_x-VOCs-aerosol chemistry. Anthropogenic emissions are based on the Global Emission Inventory Activity (GEIA) [*Benkovitz et al.*, 1996], overwritten with NO_x, CO and SO_x from the Emission Database for Global Atmospheric Research (EDGAR) inventory [*Olivier and Berdowski*, 2001] and from various regional emissions inventories as described by *Nassar et al.* [2009]. Anthropogenic emissions in Asia are from the Streets 2000 inventory [*Streets et al.*, 2003], with anthropogenic CO emissions in China updated by the Streets 2001 inventory [*Streets et al.*, 2006]. These base inventory emissions are scaled to our simulation year 2004, following *van Donkelaar et al.* [2008]. The 2004 anthropogenic emission for Asia (0–60°N, 65–150°E) is 8.0 Tg N/yr for NO_x and 173.0 Tg/yr for CO. Biofuel emissions follow *Yevich and Logan* [2003]. Biogenic VOCs emissions are based on the Model of Emissions of Gases and Aerosol from Nature (MEGAN) inventory [*Guenther et al.*, 2006]. Biomass burning emissions are based on the Global Fire Emissions Database version 2 (GFEDv2), which resolves interannual variability [*van der Werf et al.*, 2006]. The monthly GFEDv2 emissions were resampled to an 8-day time step using MODIS fire hot spots [*Giglio et al.*, 2003; *Nassar et al.*, 2009].

[70] Lightning NO_x emissions in GEOS-Chem are calculated locally in deep convection events with the scheme of *Price and Rind* [1992] that links flash rates to convective cloud top heights. The spatial distribution of lightning averaged over 11 years in the model is constrained to match the climatological (11-year) satellite observations of lightning flash rates from the Optical Transient Detector / Lightning Imaging Sensor (OTD-LIS) High Resolution Monthly Climatology (HRMC v2.2) product by applying a local monthly rescaling factor [*Sauvage et al.*, 2007; *Nassar et al.*, 2009]. The interannual variability of the lightning NO_x emissions as represented by the model is retained, with approximately 6 Tg N yr^{-1} released globally [*Sauvage et al.*, 2007; *Nassar et al.*, 2009]. The vertical distribution of lightning NO_x emissions follows *Pickering et al.* [1998], with most of NO_x in the UT (55–75% above 8 km). Transport of O_3 from the stratosphere is specified with the Synoz (synthetic O_3) scheme of *McLinden et al.* [2000] by imposing a global net cross-tropopause flux of 495 Tg O_3 per year.

References

Benkovitz, C. M., M. T. Scholtz, J. Pacyna, L. Tarrason, J. Dignon, E. C. Voldner, P. A. Spiro, J. A. Logan, and T. E. Graedel (1996), Global gridded inventories of anthropogenic emissions of sulfur and nitrogen, *J. Geophys. Res.*, *101*(D22), 29,239–29,253, doi:10.1029/96JD00126.

Bey, I., D. J. Jacob, R. M. Yantosca, J. A. Logan, B. Field, A. M. Fiore, Q. Li, H. Liu, L. J. Mickley, and M. Schultz (2001a), Global modeling of tropospheric chemistry with assimilated meteorology: Model description and evaluation, *J. Geophys. Res.*, *106*, 23,073–23,095, doi:10.1029/2001JD000807.

Bey, I., D. J. Jacob, J. A. Logan, and R. M. Yantosca (2001b), Asian chemical outflow to the Pacific in spring: Origins, pathways, and budgets, *J. Geophys. Res.*, *106*, 23,097–23,113, doi:10.1029/2001JD000806.

Chan, C. Y., and L. Y. Chan (2000), Effect of meteorology and air pollutant transport on ozone episodes at a subtropical coastal Asian city, Hong Kong, *J. Geophys. Res.*, *105*, 20,707–20,724, doi:10.1029/2000JD900140.

Chan, C. Y., L. Y. Chan, J. M. Harris, S. J. Oltmans, D. R. Blake, Y. Qin, Y. G. Zheng, and X. D. Zheng (2003a), Characteristics of biomass burning emission sources, transport, and chemical speciation in enhanced springtime tropospheric ozone profile over Hong Kong, *J. Geophys. Res.*, *108*(D1), 4015, doi:10.1029/2001JD001555.

Chan, C. Y., L. Y. Chan, W. L. Chang, Y. G. Zheng, H. Cui, X. D. Zheng, Y. Qin, and Y. S. Li (2003b), Characteristics of a tropospheric ozone profile and implications for the origin of ozone over subtropical China in the spring of 2001, *J. Geophys. Res.*, *108*(D20), 8800, doi:10.1029/2003JD003427.

Chan, C. Y., L. Y. Chan, H. Cui, X. D. Zheng, Y. G. Zheng, Y. Qin, and Y. S. Li (2003c), Origin of the springtime tropospheric ozone maximum over east China at LinAn in 2001, *Tellus, Ser. B*, *55*, 982–992.

Chan, C. Y., et al. (2004), Vertical profile and origin of wintertime tropospheric ozone over China during the PEACE-A period, *J. Geophys. Res.*, *109*, D23S06, doi:10.1029/2004JD004581.

Chan, C. Y., K. H. Wong, Y. S. Li, L. Y. Chan, and X. D. Zheng (2006), The effects of Southeast Asia fire activities on tropospheric ozone, trace gases and aerosols at a remote site over the Tibetan Plateau of southwest China, *Tellus, Ser. B*, *58*, 310–318.

Chan, C. Y., Y. S. Li, J. H. Tang, Y. K. Leung, M. C. Wu, L. Y. Chan, C. C. Chang, and S. C. Liu (2007), An analysis on abnormally low ozone in the upper troposphere over subtropical East Asia in spring 2004, *Atmos. Environ.*, *41*, 3556–3564, doi:10.1016/j.atmosenv.2007.01.004.

Chan, L. Y., H. Y. Liu, K. S. Lam, T. Wang, S. J. Oltmans, and J. M. Harris (1998), Analysis of the seasonal behavior of tropospheric ozone at Hong Kong, *Atmos. Environ.*, *32*, 159–168, doi:10.1016/S1352-2310(97)00320-8.

Cooper, O., et al. (2004), On the life cycle of a stratospheric intrusion and its dispersion into polluted warm conveyor belts, *J. Geophys. Res.*, *109*, D23S09, doi:10.1029/2003JD004006.

Cooper, O. R., et al. (2010), Increasing springtime ozone mixing ratios in the free troposphere over western North America, *Nature*, *463*, 344–348, doi:10.1038/nature08708.

Ding, A. J., T. Wang, V. Thouret, J. P. Cammas, and P. Nédélec (2008), Tropospheric ozone climatology over Beijing: Analysis of aircraft data from the MOZAIC program, *Atmos. Chem. Phys.*, *8*, 1–13, doi:10.5194/acp-8-1-2008.

Ding, Y., and J. C. L. Chan (2005), The East Asian summer monsoon: An overview, *Meteorol. Atmos. Phys.*, *89*, 117–142, doi:10.1007/s00703-005-0125-z.

Duncan, B. N., R. V. Martin, A. C. Staudt, R. Yevich, and J. A. Logan (2003), Interannual and seasonal variability of biomass burning emissions constrained by satellite observations, *J. Geophys. Res.*, *108*(D2), 4100, doi:10.1029/2002JD002378.

Fiore, A. M., D. J. Jacob, I. Bey, R. M. Yantosca, B. D. Field, A. C. Fusco, and J. G. Wilkinson (2002), Background ozone over the United States: Implications for air quality policy, *J. Geophys. Res.*, *107*(D15), 4275, doi:10.1029/2001JD000982.

Fishman, J., and V. G. Brackett (1997), The climatological distribution of tropospheric ozone derived from satellite measurements using version 7 Total Ozone Mapping Spectrometer and Stratospheric Aerosol and Gas Experiment data sets, *J. Geophys. Res.*, *102*, 19,275–19,278, doi:10.1029/97JD01373.

Giglio, L., J. Descloitres, C. O. Justice, and Y. J. Kaufman (2003), An enhanced contextual fire detection algorithm for MODIS, *Remote Sens. Environ.*, *87*, 273–282, doi:10.1016/S0034-4257(03)00184-6.

Guenther, A., T. Karl, P. Harley, C. Wiedinmyer, P. I. Palmer, and C. Geron (2006), Estimates of global terrestrial isoprene emissions using MEGAN (Model of Emissions of Gases and Aerosols from Nature), *Atmos. Chem. Phys.*, *6*, 3181–3210, doi:10.5194/acp-6-3181-2006.

Hack, J. J. (1994), Parameterization of moist convection in the NCAR community climate model (CCM2), *J. Geophys. Res.*, *99*, 5551–5568, doi:10.1029/93JD03478.

Hao, W. M., and M.-H. Liu (1994), Spatial and temporal distribution of tropical biomass burning, *Global Biogeochem. Cycles*, *8*, 495–503, doi:10.1029/94GB02086.

Harris, J. M., and J. D. W. Kahl (1994), Analysis of 10-day isentropic flow patterns for Barrow, Alaska: 1985–1992, *J. Geophys. Res.*, *99*, 25,845–25,855, doi:10.1029/94JD02324.

Honrath, R. E., A. J. Hamlin, and J. T. Merrill (1996), Transport of ozone precursors from the Arctic troposphere to the North Atlantic region, *J. Geophys. Res.*, *101*, 29,335–29,351, doi:10.1029/95JD02673.

Hsu, J., M. J. Prather, and O. Wild (2005), Diagnosing the stratosphere-to-troposphere flux of ozone in a chemistry transport model, *J. Geophys. Res.*, *110*, D19305, doi:10.1029/2005JD006045.

Hudman, R. C., et al. (2004), Ozone production in transpacific Asian pollution plumes and implications for ozone air quality in California, *J. Geophys. Res.*, *109*, D23S10, doi:10.1029/2004JD004974.

Hudman, R. C., L. T. Murray, D. J. Jacob, S. Turquety, S. Wu, D. B. Millet, M. Avery, A. H. Goldstein, and J. Holloway (2009), North American influence on tropospheric ozone and the effects of recent emission reductions: Constraints from ICARTT observations, *J. Geophys. Res.*, *114*, D07302, doi:10.1029/2008JD010126.

Jacob, D. J., J. A. Logan, and P. P. Murti (1999), Effect of rising Asian emissions on surface ozone in the United States, *Geophys. Res. Lett.*, *26*, 2175–2178, doi:10.1029/1999GL900450.

Jaffe, D., et al. (1999), Transport of Asian air pollution to North America, *Geophys. Res. Lett.*, *26*, 711–714, doi:10.1029/1999GL900100.

Jourdain, L., et al. (2010), Lightning NO_x emissions over the USA constrained by TES ozone observations and the GEOS-Chem model, *Atmos. Chem. Phys.*, *10*, 107–119, doi:10.5194/acp-10-107-2010.

Lacis, A. A., D. J. Wuebbles, and J. A. Logan (1990), Radiative forcing of climate by changes in the vertical distribution of ozone, *J. Geophys. Res.*, *95*(D7), 9971–9981, doi:1029/JD095iD07p09971.

Lelieveld, J., and F. J. Dentener (2000), What controls tropospheric ozone?, *J. Geophys. Res.*, *105*, 3531–3551, doi:10.1029/1999JD901011.

Li, Q., D. J. Jacob, J. A. Logan, I. Bey, R. M. Yantosca, H. Y. Liu, R. V. Martin, A. M. Fiore, B. D. Field, and B. N. Duncan (2001), A tropospheric ozone maximum over the Middle East, *Geophys. Res. Lett.*, *28*, 3235–3238, doi:10.1029/2001GL013134.

Li, Q., D. J. Jacob, T. D. Fairlie, H. Liu, R. V. Martin, and R. M. Yantosca (2002), Stratospheric versus pollution influences on ozone at Bermuda: Reconciling past analyses, *J. Geophys. Res.*, *107*(D22), 4611, doi:10.1029/2002JD002138.

Li, Q., et al. (2005), Convective outflow of South Asian pollution: A global CTM simulation compared with EOS MLS observations, *Geophys. Res. Lett.*, *32*, L14826, doi:10.1029/2005GL022762.

Lin, C. Y., H. M. Hsu, Y. H. Lee, C. H. Kuo, Y. F. Sheng, and D. A. Chu (2009), A new transport mechanism of biomass burning from Indochina as identified by modeling studies, *Atmos. Chem. Phys.*, *9*, 7901–7911, doi:10.5194/acp-9-7901-2009.

Lin, C. Y., C. C. Chang, C. Y. Chan, C. H. Kuo, W. C. Chen, D. A. Chu, and S. C. Liu (2010), Characteristics of springtime profiles and sources of ozone in the low troposphere over northern Taiwan, *Atmos. Environ.*, *44*, 182–193, doi:10.1016/j.atmosenv.2009.10.020.

Lin, J. T. (2012), Satellite constraint for emissions of nitrogen oxides from anthropogenic, lightning and soil sources over east China on a high-resolution grid, *Atmos. Chem. Phys.*, *12*, 2881–2898, doi:10.5194/acp-12-2881-2012.

Lin, J. T., and M. B. McElroy (2010), Impact of boundary mixing on pollutant vertical profiles in the lower troposphere: Implications to satellite remote sensing, *Atmos. Environ.*, *44*, 1726–1739, doi:10.1016/j.atmosenv.2010.02.009.

Lin, M., T. Holloway, G. R. Carmichael, and A. M. Fiore (2010), Quantifying pollution inflow and outflow over East Asia in spring with regional and global models, *Atmos. Chem. Phys.*, *10*, 4221–4239, doi:10.5194/acp-10-4221-2010.

Lin, M., et al. (2012), Transport of Asian ozone pollution into surface air over the western United States in spring, *J. Geophys. Res.*, *117*, D00V07, doi:10.1029/2011JD016961.

Liu, C. M., and H. W. Chang (2001), Characteristics of tropospheric column ozone over Taiwan, *Terr. Atmos. Oceanic Sci.*, *12*, 365–376.

Liu, H., W. L. Chang, S. Oltmans, L. Y. Chan, and J. M. Harris (1999), On springtime high ozone events in the lower troposphere from Southeast Asian biomass burning, *Atmos. Environ.*, *33*, 2403–2410, doi:10.1016/S1352-2310(98)00357-4.

Liu, H., D. J. Jacob, L. Y. Chan, S. J. Oltmans, I. Bey, R. M. Yantosca, J. M. Harris, B. N. Duncan, and R. V. Martin (2002), Sources of tropospheric ozone along the Asian Pacific Rim: An analysis of ozonesonde observations, *J. Geophys. Res.*, *107*(D21), 4573, doi:10.1029/2001JD002005.

Liu, H., D. J. Jacob, I. Bey, R. M. Yantosca, B. N. Duncan, and G. W. Sachse (2003), Transport pathways for Asian pollution outflow over the Pacific: Interannual and seasonal variations, *J. Geophys. Res.*, *108*(D20), 8786, doi:10.1029/2002JD003102.

Liu, J. J., D. B. A. Jones, J. R. Worden, D. Noone, M. Parrington, and J. Kar (2009), Analysis of the summertime buildup of tropospheric ozone abundances over the Middle East and North Africa as observed by the Tropospheric Emission Spectrometer instrument, *J. Geophys. Res.*, *114*, D05304, doi:10.1029/2008JD010993.

Liu, S., M. Trainer, F. Fehsenfeld, D. Parrish, E. Williams, D. Fahey, G. Hubler, and P. Murphy (1987), Ozone production in the rural troposphere and the implications for regional and global ozone distributions, *J. Geophys. Res.*, *92*, 4191–4207, doi:10.1029/JD092iD04p04191.

Logan, J. A. (1985), Tropospheric ozone: Seasonal behavior, trends, and anthropogenic influence, *J. Geophys. Res.*, *90*, 10,463–10,482, doi:10.1029/JD090iD06p10463.

Logan, J. (1999), An analysis of ozonesonde data for the troposphere: Recommendations for testing 3-D models and development of a gridded climatology for tropospheric ozone, *J. Geophys. Res.*, *104*(D13), 16,115–16,149, doi:10.1029/1998JD100096.

Martin, R. V., et al. (2002), Interpretation of TOMS observations of tropical tropospheric ozone with a global model and in-situ observations, *J. Geophys. Res.*, *107*(D18), 4351, doi:10.1029/2001JD001480.

McLinden, C. A., S. C. Olsen, B. Hannegan, O. Wild, M. J. Prather, and J. Sundet (2000), Stratospheric ozone in 3-D models: A simple chemistry and the cross-tropopause flux, *J. Geophys. Res.*, *105*, 14,653–14,665, doi:10.1029/2000JD900124.

Monks, P. S. (2000), A review of the observations and origins of the spring ozone maximum, *Atmos. Environ.*, *34*, 3545–3561, doi:10.1016/S1352-2310(00)00129-1.

Nassar, R., J. A. Logan, I. A. Megretskaia, L. T. Murray, L. Zhang, and D. B. A. Jones (2009), Analysis of tropical tropospheric ozone, carbon monoxide, and water vapor during the 2006 El Niño using TES observations and the GEOS-Chem model, *J. Geophys. Res.*, *114*, D17304, doi:10.1029/2009JD011760.

Olivier, J. G. J., and J. J. M. Berdowski (2001), Global emissions source and sinks, in *The Climate System*, edited by J. Berdowski, R. Guicherit, and B. J. Heji, pp. 33–78, A. A. Balkema, Lisse, Netherlands.

Oltmans, S. J., and H. Levy II (1992), Seasonal cycle of surface ozone over the western North Atlantic, *Nature*, *358*, 392–394, doi:10.1038/358392a0.

Oltmans, S. J., et al. (1996), Summer and spring ozone profiles over the North Atlantic from ozonesonde measurements, *J. Geophys. Res.*, *101*, 29,179–29,200, doi:10.1029/96JD01713.

Oltmans, S. J., et al. (2004), Tropospheric ozone over the North Pacific from ozonesonde observations, *J. Geophys. Res.*, *109*, D15S01, doi:10.1029/2003JD003466.

Park, R. J., D. J. Jacob, B. D. Field, R. M. Yantosca, and M. Chin (2004), Natural and transboundary pollution influences on sulfate-nitrate-ammonium aerosols in the United States: Implications for policy, *J. Geophys. Res.*, *109*, D15204, doi:10.1029/2003JD004473.

Parrington, M., D. B. A. Jones, K. W. Bowman, L. W. Horowitz, A. M. Thompson, D. W. Tarasick, and J. C. Witte (2008), Estimating the summertime tropospheric ozone distribution over North America through assimilation of observations from the Tropospheric Emission Spectrometer, *J. Geophys. Res.*, *113*, D18307, doi:10.1029/2007JD009341.

Penkett, S. A., and K. A. Brice (1986), The spring maximum in photooxidants in the Northern Hemisphere troposphere, *Nature*, *319*, 655–657, doi:10.1038/319655a0.

Pickering, K. E., Y. Wang, W.-K. Tao, C. Price, and J.-F. Müller (1998), Vertical distributions of lightning NO_x for use in regional and global chemical transport models, *J. Geophys. Res.*, *103*, 31,203–31,216, doi:10.1029/98JD02651.

Price, C., and D. Rind (1992), A simple lightning parameterization for calculating global lightning distributions, *J. Geophys. Res.*, *97*, 9919–9933, doi:10.1029/92JD00719.

Ramanathan, V., and R. E. Dickinson (1979), Role of stratospheric ozone in the zonal and seasonal radiative energy balance of the Earth-troposphere system, *J. Atmos. Sci.*, *36*, 1084–1104.

Richter, A., J. P. Burrows, H. Nüß, C. Granier, and U. Niemeier (2005), Increase in tropospheric nitrogen dioxide over China observed from space, *Nature*, *437*, 129–132, doi:10.1038/nature04092.

Robinson, R. D. (1980), The transport of minor atmospheric constituents between troposphere and stratosphere, *Q. J. R. Meteorol. Soc.*, *106*, 227–253, doi:10.1002/qj.49710644802.

Sauvage, B., R. V. Martin, A. van Donkelaar, X. Liu, K. Chance, L. Jaeglé, P. I. Palmer, S. Wu, and T.-M. Fu (2007), Remote sensed and in situ constraints on processes affecting tropical tropospheric ozone, *Atmos. Chem. Phys.*, *7*, 815–838, doi:10.5194/acp-7-815-2007.

Schenkel, A., and B. Broder (1982), Interference of some trace gases with ozone measurement by the KI-Method, *Atmos. Environ.*, *16*, 2187–2190, doi:10.1016/0004-6981(82)90289-X.

Smit, H. G. J., and W. Sträter (2004), JOSIE-1998 performance of the ECC ozone sondes of SPC-6A and ENSCI-Z type, *WMO/TD-No. 1218*, WMO, Geneva, Switzerland.

Stohl, A., et al. (2003), Stratosphere-troposphere exchange: A review, and what we have learned from STACCATO, *J. Geophys. Res.*, *108*(D12), 8516, doi:10.1029/2002JD002490.

Streets, D. G., et al. (2003), An inventory of gaseous and primary aerosol emissions in Asia in the year 2000, *J. Geophys. Res.*, *108*(D21), 8809, doi:10.1029/2002JD003093.

Streets, D. G., Q. Zhang, L. Wang, K. He, J. Hao, Y. Wu, Y. Tang, and G. R. Carmichael (2006), Revisiting China's CO emissions after the Transport and Chemical Evolution over the Pacific (TRACE-P) mission: Synthesis of inventories, atmospheric modeling, and observations, *J. Geophys. Res.*, *111*, D14306, doi:10.1029/2006JD007118.

Sudo, K., and H. Akimoto (2007), Global source attribution of tropospheric ozone: Long-range transport from various source regions, *J. Geophys. Res.*, *112*, D12302, doi:10.1029/2006JD007992.

Thompson, A. M. (1992), The oxidizing capacity of the Earth's atmosphere: Probable past and future changes, *Science*, *256*, 1157–1165, doi:10.1126/science.256.5060.1157.

van der Werf, G. R., J. T. Randerson, L. Giglio, G. J. Collatz, P. S. Kasibhatla, and A. F. Arellano Jr. (2006), Interannual variability in global biomass burning emissions from 1997 to 2004, *Atmos. Chem. Phys.*, *6*, 3423–3441, doi:10.5194/acp-6-3423-2006.

van Donkelaar, A., et al. (2008), Analysis of aircraft and satellite measurements from the Intercontinental Chemical Transport Experiment (INTEX-B) to quantify long-range transport of East Asian sulfur to Canada, *Atmos. Chem. Phys.*, *8*, 2999–3014, doi:10.5194/acp-8-2999-2008.

Wang, T., A. J. Ding, D. R. Blake, W. Zahorowski, C. N. Poon, and Y. S. Li (2003), Chemical characterization of the boundary layer outflow of air pollution to Hong Kong during February–April 2001, *J. Geophys. Res.*, *108*(D20), 8787, doi:10.1029/2002JD003272.

Wang, T., et al. (2004), Relationships of trace gases and aerosols and the emission characteristics at Lin'an, a rural site in eastern China, during spring 2001, *J. Geophys. Res.*, *109*, D19S05, doi:10.1029/2003JD004119.

Wang, T., X. L. Wei, A. J. Ding, C. N. Poon, K. S. Lam, Y. S. Li, L. Y. Chan, and M. Anson (2009), Increasing surface ozone concentrations in the background atmosphere of southern China, 1994–2007, *Atmos. Chem. Phys.*, *9*, 6217–6227, doi:10.5194/acp-9-6217-2009.

Wang, Y., D. J. Jacob, and J. A. Logan (1998), Global simulation of tropospheric O_3-NO_x-hydrocarbon chemistry: 3. Origin of tropospheric ozone and effects of nonmethane hydrocarbons, *J. Geophys. Res.*, *103*, 10,757–10,767, doi:10.1029/98JD00156.

Yevich, R., and J. A. Logan (2003), An assessment of biofuel use and burning of agricultural waste in the developing world, *Global Biogeochem. Cycles*, *17*(4), 1095, doi:10.1029/2002GB001952.

Yienger, J. J., M. Galanter, T. A. Holloway, M. J. Phadnis, S. K. Guttikunda, G. R. Carmichael, W. J. Moxim, and H. Levy II (2000), The episodic nature of air pollution transport from Asia to North America, *J. Geophys. Res.*, *105*, 26,931–26,945, doi:10.1029/2000JD900309.

Zhang, G. J., and N. A. McFarlane (1995), Sensitivity of climate simulations to the parameterization of cumulus convection in the Canadian Climate Centre general circulation model, *Atmos. Ocean*, *33*, 407–446, doi:10.1080/07055900.1995.9649539.

Zhang, L., et al. (2008), Transpacific transport of ozone pollution and the effect of recent Asian emission increases on air quality in North America: An integrated analysis using satellite, aircraft, ozonesonde, and surface observations, *Atmos. Chem. Phys.*, *8*, 6117–6136, doi:10.5194/acp-8-6117-2008.

Zhang, L., Q. B. Li, J. Jin, H. Liu, N. Livesey, J. H. Jiang, Y. Mao, D. Chen, M. Luo, and Y. Chen (2011), Impacts of 2006 Indonesian fires and dynamics on tropical upper tropospheric carbon monoxide and ozone, *Atmos. Chem. Phys.*, *11*, 10,929–10,946, doi:10.5194/acp-11-10929-2011.

Zheng, X. D., X. J. Zhou, J. Tang, Y. Qin, and C. Y. Chan (2004), A meteorological analysis on a low tropospheric ozone event over Xining, northwestern China on 26–27 July 1996, *Atmos. Environ.*, *38*, 261–271, doi:10.1016/j.atmosenv.2003.09.063.